NASA/TP-20260002311

Microstructural Evolution and Mechanical Properties of LP-DED NASA HR-1 – A Hydrogen Resistant AM Superalloy for Space Propulsion Applications

P.S. Chen,
Amentum ESSCA Group, Huntsville, Alabama

C.H. Su, C.C. Katsarelis, P.R. Gradl
Marshall Space Flight Center, Huntsville, Alabama

A. Garg
University of Toledo, Toledo, Ohio

A.G. Culver
Amentum ESSCA Group, Huntsville, Alabama

P.W.C. Northrop
CFD Research Corporation, Amentum ESSCA Group, Huntsville, Alabama

March 2026

The NASA STI Program…in Profile

The NASA STI Program collects, organizes, provides for archiving, and disseminates NASA's STI. The NASA STI program provides access to the NTRS Registered and its public interface, the NASA Technical Reports Server, thus providing one of the largest collections of aeronautical and space science STI in the world. Results are published in both non-NASA channels and by NASA in the NASA STI Report Series, which includes the following report types:

- TECHNICAL PUBLICATION. Reports of completed research or a major significant phase of research that present the results of NASA programs and include extensive data or theoretical analysis. Includes compilations of significant scientific and technical data and information deemed to be of continuing reference value. NASA's counterpart of peer- reviewed formal professional papers but has less stringent limitations on manuscript length and extent of graphic presentations.

- TECHNICAL MEMORANDUM. Scientific and technical findings that are preliminary or of specialized interest, e.g., quick release reports, working papers, and bibliographies that contain minimal annotation. Does not contain extensive analysis.

- CONTRACTOR REPORT. Scientific and technical findings by NASA-sponsored contractors and grantees.

- CONFERENCE PUBLICATION. Collected papers from scientific and technical conferences, symposia, seminars, or other meetings sponsored or cosponsored by NASA.

- SPECIAL PUBLICATION. Scientific, technical, or historical information from NASA programs, projects, and mission, often concerned with subjects having substantial public interest.

- TECHNICAL TRANSLATION. English-language translations of foreign scientific and technical material pertinent to NASA's mission.

Specialized services also include organizing and publishing research results, distributing specialized research announcements and feeds, providing information desk and personal search support, and enabling data exchange services.

For more information about the NASA STI program, see the following:

- Access the NASA STI program home page at http://www.sti.nasa.gov

- Help desk contact information:
  https://www.sti.nasa.gov/sti-contact-form/
  and select the "General" help request type.

NASA/TP–20260002311

Microstructural Evolution and Mechanical Properties of LP-DED NASA HR-1 – A Hydrogen Resistant AM Superalloy for Space Propulsion Applications

P.S. Chen,
Amentum ESSCA Group, Huntsville, Alabama

C.H. Su, C.C. Katsarelis, P.R. Gradl
Marshall Space Flight Center, Huntsville, Alabama

A. Garg
University of Toledo, Toledo, Ohio

A.G. Culver
Amentum ESSCA Group, Huntsville, Alabama

P.W.C. Northrop
CFD Research Corporation, Amentum ESSCA Group, Huntsville, Alabama

National Aeronautics and
Space Administration

Marshall Space Flight Center • Huntsville, Alabama 35812

March 2026

TRADEMARKS

Available from: NASA STI Information Desk
Mail Stop 148
NASA Langley Research Center
Hampton, VA 23681–2199, USA
757–864–9658

Table of Contents

List of Figures

List of Tables

List of Abbreviations, Acronyms, and Symbols

μin	microinches
Al	Aluminum
AM	Additive manufacturing
DSC	differential scanning calorimetry
EDS	energy-dispersive X-ray spectroscopy
FCC	face-centered cubic
Fe	Iron
FFT	Fast Fourier Transform
GH_2	gaseous hydrogen
GHe	gaseous helium
GRC	Glenn Research Center
HCF	high cycle fatigue
HEE	hydrogen environment embrittlement
HR-1	Hydrogen Resistant-1
HRC	Rockwell Hardness C
HRTEM	high-resolution transmission electron microscopy
kN	kilonewton
ksi	kilopound force per square inch
LCF	low-cycle fatigue
LP-DED	laser powder directed energy deposition
LRE	liquid rocket engine
LSG	low-stress grinding

NASA	National Aeronautics and Space Administration
Ni	nickel
Ra	arithmetic mean surface roughness
RMS	root mean square
RPMI	RMP Innovations Inc.
SAED	selected area electron diffraction
SEM	scanning electron microscopy
STEM-HAADF	scanning transmission electron microscopy high-angle annular dark-field
TEM	transmission electron microscopy
Ti	titanium
UTS	ultimate tensile strength
wt%	weight percentage
YS	yield strength

TECHNICAL PUBLICATION

Microstructural Evolution and Mechanical Properties of LP-DED NASA HR-1 – A Hydrogen Resistant AM Superalloy for Space Propulsion Applications

1. INTRODUCTION

The National Aeronautics and Space Administration (NASA) has actively pursued metal additive manufacturing (AM) technologies for spaceflight applications since the late 2000s. AM offers transformative advantages in cost, schedule, part consolidation, and design flexibility. Among the various AM techniques, laser powder directed energy deposition (LP-DED) is particularly well suited for fabricating complex geometries with fine feature resolution.
In propulsion systems that utilize high-pressure gaseous hydrogen—such as liquid hydrogen rocket engines—hydrogen environment embrittlement (HEE) presents a serious threat to material performance[1,2]. Mechanical property degradation under these conditions can compromise component reliability, especially under cyclic loading.

To address this challenge, NASA developed NASA HR-1 (Hydrogen Resistant-1) as a solution for liquid rocket engine components operating in hydrogen-rich environments, using the LP-DED technique[3-9]. A key component in a liquid rocket engine is the exhaust nozzle, which is typically regeneratively cooled (regen) due to the high heat flux. NASA HR-1 was specifically developed for regen nozzle applications using hydrogen as a propellant, providing resistance to HEE, a critical issue for many materials. The AM version of NASA HR-1 was also formulated to achieve high ultimate tensile strength, along with high yield strength and ductility in this environment[5,6]. Low-cycle fatigue (LCF) is another important consideration in nozzle design, as components are expected to endure multiple starts and missions. Additionally, the LP-DED version of the alloy exhibits improved thermal conductivity compared to its wrought counterpart, which benefits nozzle cooling. Overall, NASA HR-1 offers an excellent balance of high strength, HEE resistance, LCF performance, thermal conductivity, and ductility to meet the demanding requirements of channel-cooled nozzles and other components used with hydrogen and other propellants.

The LP-DED–processed NASA HR-1 requires several post-processing heat treatment steps to achieve the material properties desirable for its intended application[6]. These steps include stress relief, homogenization, solution annealing, and aging for precipitation hardening. The stress relief treatment mitigates residual stresses accumulated during the LP-DED process and minimizes the potential for distortion. Homogenization, a common step for AM materials, reduces elemental segregation and promotes recrystallization to develop a more equiaxed grain structure. The subsequent solution annealing treatment heats the part to a solid solution temperature to dissolve the undesirable η-phase that forms during cooling from homogenization, followed by rapid cooling to retain an η-phase–free microstructure. Finally, aging promotes precipitation of the strengthening γ′ phase in the alloy.

The integration of compositional design and optimized thermal processing enables high-quality LP-DED NASA HR-1 components with excellent microstructural and mechanical stability. Improved chemical and microstructure homogeneity enhances ductility and fatigue resistance—both critical for safe and reliable operation in high-pressure hydrogen environments. NASA has successfully fabricated and hot-fire tested multiple subscale and full-scale channel wall nozzles using LP-DED NASA HR-1 [5,6, 9-14]. These efforts included process refinements to support thin-wall construction and various channel geometries.

Throughout development, several key observations emerged. After homogenization, the as-built columnar grain structure transforms into a fully equiaxed microstructure. However, subsequent treatments—such as solution annealing and aging—result in changes that are more difficult to track. The grain structure remains largely unchanged, and the γ′ precipitates, typically 5–10 nm in diameter, are beyond the resolution of scanning electron microscopy (SEM). While transmission electron microscopy (TEM) can resolve these fine precipitates, TEM sample preparation is time-consuming and difficult for LP-DED material. As an alternative, differential scanning calorimetry (DSC) offers a useful, qualitative approach to monitor precipitate evolution throughout different stages of heat treatment.

The overall goal is to improve the understanding of how heat treatment affects the microstructure and mechanical performance of LP-DED NASA HR-1. This paper presents heat treatment design considerations, microstructural characterization, mechanical testing – including tensile and LCF testing in both air and hydrogen environments.

2. EXPERIMENTAL PROCEDURES AND METHODS

2.1 Material and Laser Powder Directed Energy Deposition (LP-DED) Process

The material used in this study consisted of multi-pass LP-DED NASA HR-1 round bars deposited using an RPM Innovations (RPMI) system. The feedstock powder for the LP-DED process was pre-alloyed, rotary-atomized NASA HR-1 powder produced by vacuum or inert induction melting, followed by rotary atomization in argon. The nominal chemical composition and specification of the NASA HR-1 powder are provided in Table 1. The powder size distribution ranged from 45 to 105 μm (–140 mesh/+325 mesh). The NASA HR-1 powder exhibited mostly spherical morphology, with some oblong ellipsoidal particles and occasional satellite particles. A representative SEM image showing the typical powder morphology used in the LP-DED process is presented in Figure 1.

LP-DED NASA HR-1 samples for heat treatment optimization and mechanical testing were deposited to a length of 4 inches and a diameter of 0.6 inches, using a laser power of 1070 watts. An illustration of the NASA HR-1 round bar fabrication process and the deposited samples is shown in Figure 2.

Table 1. Nominal chemical composition (wt%) of NASA HR-1 powder and its specification limits.

Element	Specification (wt%)		
	Nominal	Minimum	Maximum
Iron	BAL	-	-
Nickel	34	33.7	34.3
Chromium	14.6	14.3	14.9
Cobalt	3.8	3.6	4
Molybdenum	1.8	1.6	2
Tungsten	1.6	1.4	1.8
Titanium	2.4	2.2	2.6
Vanadium	0.3	0.28	0.32
Aluminum	0.25	0.23	0.27
Sulfur	-	-	0.005
Phosphorus	-	-	0.005
Carbon	-	-	0.03
Silicon	-	-	0.05
Boron	-	-	0.005
Manganese	-	-	0.05
Hydrogen	-	-	<50 ppm
Oxygen	-	-	<100 ppm (-140/+325 mesh) <200 ppm (-325 mesh/+10 um)
Nitrogen	-	-	<50 ppm

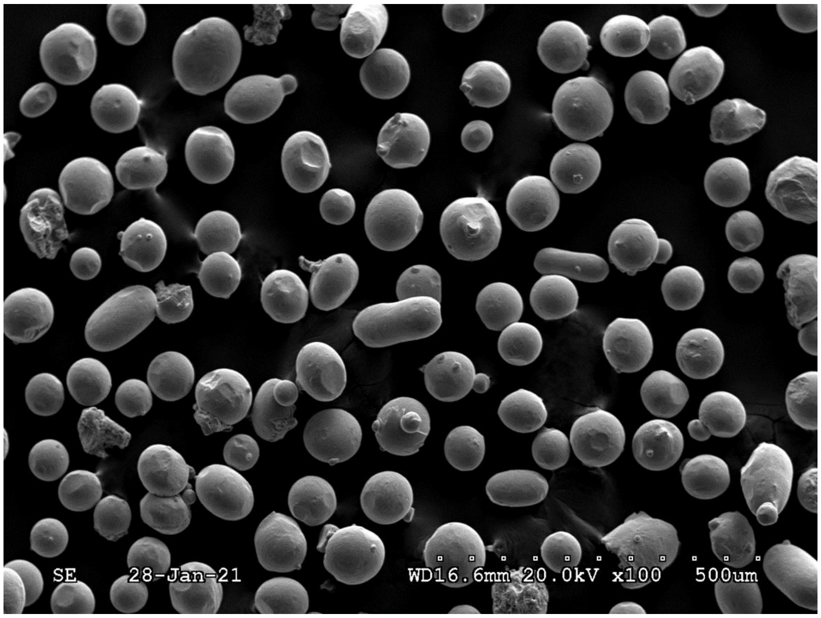

Figure 1. A SEM image showing the morphology of NASA HR-1 powder particles.

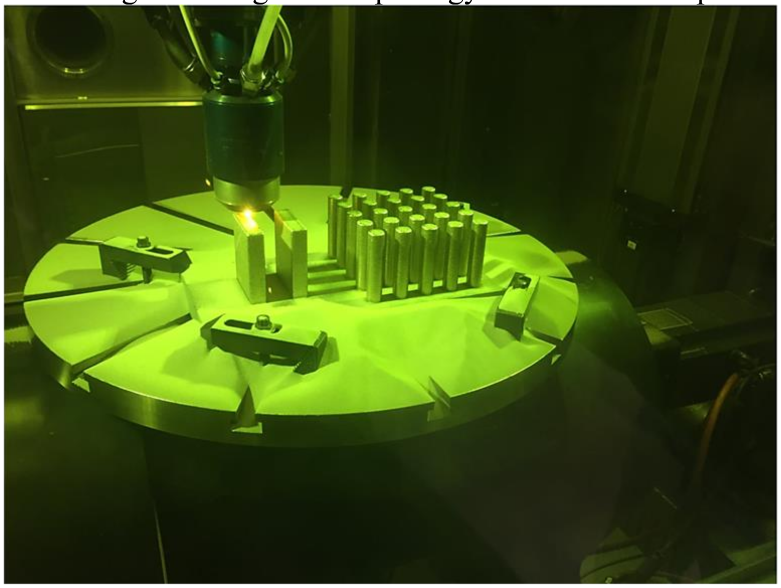

(a)

(b)

Figure 2. (a) Illustration of NASA HR-1 round bar fabrication via the LP-DED process; (b) round bars measuring 4 inches in length and 0.6 inches in diameter, fabricated at a laser power of 1070 watts using virgin powder from lot HRA13.

2.2 Heat Treatment

After deposition, the round bar samples required post-processing heat treatment to achieve the desired material properties. The heat treatment sequence included stress relief, homogenization, solution annealing, and aging. The as-built samples first underwent stress relief at 1950 °F (1065.56 °C) for 1.5 hours, followed by slow furnace cooling. Afterward, the samples were homogenized at 2125 °F (1162.78 °C) for 6 hours in a vacuum furnace. At the end of homogenization, the samples were argon quenched to minimize η-phase precipitation. Next, the samples were solution annealed at 1950 °F (1065.56 °C) for 1 hour in vacuum, followed by an argon quench. This was followed by a two-step aging treatment at 1275 °F (690.56 °C) for 16 hours and 1150 °F (621.11 °C) for 16 hours (a total of 32 hours) in a vacuum furnace to complete the heat treatment process[6].

2.3 Differential Scanning Calorimetry (DSC)

DSC was used to analyze the melting and solidification behavior of LP-DED NASA HR-1. DSC analyses were performed on virgin NASA HR-1 powder and as-built LP-DED bars using a TA SDT Q600 thermal analyzer. The tests were conducted in a high-purity argon atmosphere, with an Al_2O_3 empty crucible used as the reference. Samples were heated from room temperature to 2732 °F (1500 °C) at a rate of 68 °F/min (20 °C/min), then cooled at the same rate down to 1112 °F (600 °C). Endothermic peaks indicate melting reactions, while exothermic peaks correspond to solidification. The objective of the DSC analysis was to gain a better understanding of the melting/solidification characteristics and phase transformation behaviors during heat treatment of LP-DED NASA HR-1.

2.4 Metallography, Scanning Electron Microscopy (SEM), and Transmission Electron Microscopy (TEM) Analyses

Selected LP-DED NASA HR-1 specimens were metallurgically characterized following heat treatment and mechanical testing. Specimens were sectioned, mounted, ground, and polished using standard metallographic procedures, which included a series of 220–2000 grit abrasive papers, followed by polishing with a 3 µm diamond suspension and 0.05 µm alumina pads. Chemical etching was performed using waterless Kalling's reagent with an immersion time of 5–10 seconds. The microstructures of both as-deposited and heat-treated NASA HR-1 samples were examined using optical microscopy (Leica DMi8 A) and scanning electron microscopy (SEM, Hitachi S-3700N) equipped with an energy-dispersive X-ray spectroscopy (EDS) detector (Oxford Instruments X-maxN 80). High-resolution optical montage images were captured to document the microstructure across the entire sample.

TEM thin foils were prepared using a twin-jet electropolishing unit with an electrolyte of 10% perchloric acid and 90% methanol (by volume), operated at 14 °F (–10 °C) and 18 V. TEM analysis was performed on two sets of LP-DED NASA HR-1 samples using a Thermo Talos F200S TEM at the High Temperature and Smart Alloy Branch, NASA Glenn Research Center (GRC). The first set was aged using a single-step cycle at 1325 °F (718.33 °C) for 16 hours (higher strength, lower ductility), while the second set underwent a two-step aging cycle at 1275 °F (690.56 °C) for 16 hours plus 1150 °F (621.11 °C) for 16 hours (lower strength, higher ductility). The primary objective of the TEM analysis was to examine the effects of aging treatment on the size, morphology, and distribution of γ' precipitates in LP-DED NASA HR-1.

2.5 Mechanical Testing

Tensile testing was performed in ambient air at a strain rate of 0.5 in/in/min over a temperature range from –320 °F (–195.56 °C) to 1400 °F (760 °C). Elevated-temperature tensile testing was conducted using a Mayes elevated-temperature extensometer (Model: R3/8 Block 2) on an Instron load frame equipped with a 250 kN load cell, following the guidelines of ASTM E21, Standard Test Methods for Elevated Temperature Tension Tests of Metallic Materials. Room-temperature testing was performed on an Instron 5582 load frame with a 100 kN load cell and an Instron Model 2620 extensometer, in accordance with ASTM E8, Standard Test Methods for Tension Testing of Metallic Materials.

Tensile testing was also conducted in 5 ksi high-pressure gaseous hydrogen (GH_2) and helium (GHe) environments at ambient temperature. The geometry of the smooth tensile specimens used for testing in both ambient air and GH_2 environments is shown in Figure 3. The specimens featured a uniform gauge section, 0.25 inch in diameter and 1.25 inches in length. Final machining of the gauge section for specimens tested in hydrogen was performed by low-stress grinding per ASTM G142. The specified surface finish (arithmetic mean surface roughness [Ra]) was 32 µin or better.

Smooth tensile testing in hydrogen was performed at a pre-yield strain rate of 0.005 in/in/min to failure. Fracture elongation was determined by measuring the change in distance between the 1-inch gauge punch marks before and after testing. HEE susceptibility was evaluated by the relative fracture elongation, defined as the ratio of fracture elongation in high-pressure GH_2 to that in ambient air.

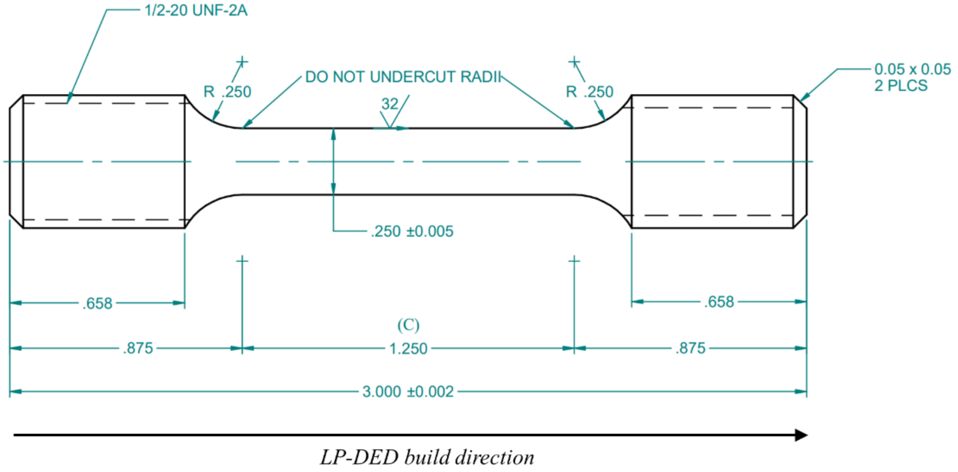

Figure 3. Geometry and dimensions of the smooth tensile specimen used for testing in ambient air and in 5 ksi gaseous hydrogen at ambient temperature. All dimensions are in inches. For specimens tested in hydrogen, the specified surface finish (Ra) on the gauge section is 32 µin or better. Low-stress grinding (LSG) was used to achieve the required surface finish.

Fully reversed tension-compression ($R = -1$) LCF tests were conducted in air at ambient temperature under strain-controlled conditions. Tests were performed at a frequency of 0.5 Hz (30 cycles per minute) and at two total strain amplitudes: 1.0% and 2.0%. Additional LCF tests were conducted in a 5 ksi high-pressure gaseous hydrogen (GH_2) environment at ambient temperature to investigate the effect of hydrogen on the LCF behavior of LP-DED NASA HR-1. These tests were also performed at $R = -1$ and at the same strain amplitudes (1.0% and 2.0%). The geometry of the LCF specimen used for both air and GH_2 testing is shown in Figure 4. The specimens had a nominal gauge diameter of 0.25 inches, and the gauge section was finish-machined using low-stress grinding. A final longitudinal polish was applied to remove circumferential machining marks and achieve a surface finish of approximately 4 µin (RMS) .

All LCF testing was conducted in accordance with ASTM E606, *Standard Test Method for Strain-Controlled Fatigue Testing*.

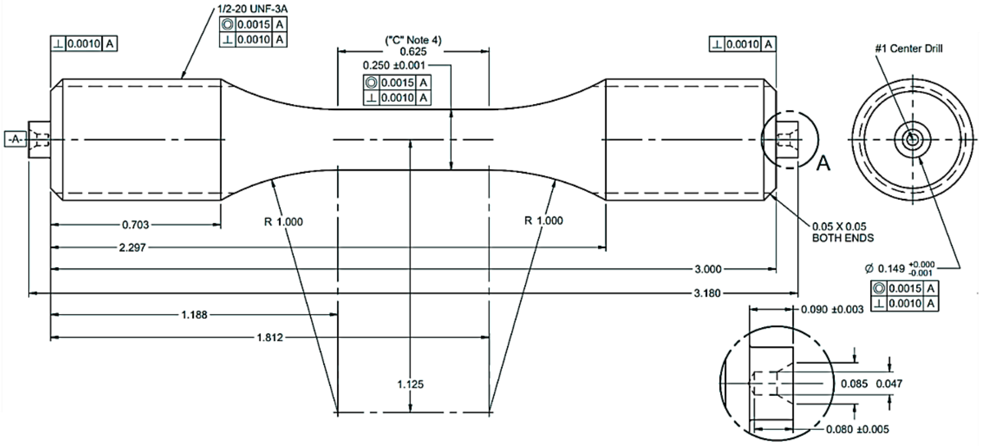

Figure 4. Geometry of the smooth specimen used for LCF testing in air and in a 5 ksi gaseous hydrogen environment at ambient temperature. All dimensions are in inches. The reduced section (C) was finished to final diameter using low-stress grinding. The specified surface finish (Ra) on the gauge section is 4 µin or better. Low-stress grinding (LSG) was used to achieve the required surface finish.

3. RESULTS AND DISCUSSION

3.1 Phase Diagram

The isopleth phase diagram of NASA HR-1, calculated using Thermo-Calc, is shown in Figure 5. An isopleth represents a vertical section through a multicomponent phase diagram in which all component concentrations are held constant except for one — in this case, titanium (Ti), which varies from 2.0 to 3.0 wt%. The base composition of NASA HR-1 is nickel-rich (Ni ~34 wt%), with a balance of iron (Fe) and other alloying elements. This isopleth was constructed to evaluate the effect of Ti content on phase stability and to aid in heat treatment design.

Figure 5 illustrates the evolution of the equilibrium phase assemblage as a function of temperature and Ti content. At high temperatures, the γ phase (face-centered cubic [FCC]) is the stable matrix phase. However, as the alloy cools, secondary phases such as the η phase (Ni_3Ti) may form. The η phase is an intermetallic compound known for its brittleness, which can be detrimental to mechanical performance, especially in hydrogen-rich environments where ductility and toughness are critical.

The diagram shows that, under equilibrium conditions, the η phase becomes stable upon cooling below ~2000 °F (1093.33 °C) when the Ti content exceeds approximately 2.4 wt%. This suggests that LP-DED NASA HR-1, especially when processed near the upper end of the Ti range, is prone to η-phase formation in the as-built condition due to non-equilibrium solidification and elemental segregation. The presence of η phase in the microstructure can reduce ductility, low-cycle fatigue resistance, and HEE resistance.

During post-processing heat treatment, particularly the solution annealing step, the objective is to fully dissolve any η phase formed during solidification or intermediate thermal processing back into the γ matrix. The isopleth indicates that for compositions near 2.4 wt% Ti, a solution annealing temperature above 2000 °F (1093.33 °C) is required to fully eliminate the η phase. This insight directly informs the selection of solution annealing parameters during heat treatment optimization.

Overall, the isopleth phase diagram serves as a valuable tool for interpreting microstructure evolution, predicting phase stability, and guiding heat treatment strategies for LP-DED NASA HR-1 components.

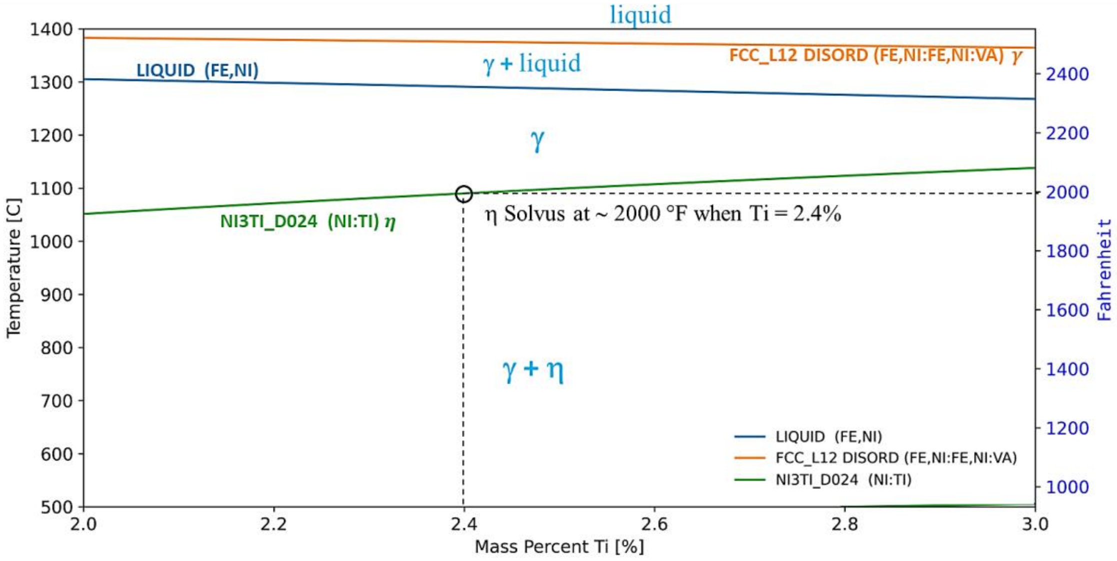

Figure 5. Isopleth phase diagram of NASA HR-1 as a function of titanium (Ti) content (2.0–3.0 wt%) at nominal composition (Nickel ~34 wt%, iron balance). All other alloying elements are fixed as specified in Table 1.

3.2 Melting and Solidification Characteristics

DSC was used to analyze the melting and solidification behavior of LP-DED NASA HR-1. Figure 6(a) shows the heating and cooling DSC curves for as-built LP-DED NASA HR-1. During heating, the material exhibits a noticeable change in heat flow beginning around 2444 °F (1340 °C), indicating the onset of melting. A distinct endothermic peak appears at 2539 °F (1393 °C), corresponding to the liquidus temperature during heating.

During the cooling cycle, a prominent exothermic peak is observed at 2453 °F (1345 °C), representing the solidus temperature upon cooling. In addition, a smaller exothermic peak appears at 2323 °F (1273 °C), corresponding to terminal liquid solidification. A close-up view of this terminal solidification event is shown in Figure 6(b). The terminal liquid begins to solidify at approximately 2368 °F (1298 °C) and completes solidification near 2260 °F (1238 °C).

The ~100 °F (~55 °C) range between the onset of melting and the peak liquidus temperature during heating suggests a relatively narrow melting window for LP-DED NASA HR-1. In contrast, the ~190 °F (~105 °C) spread between the solidus and terminal solidification temperatures during cooling indicates a moderately wide solidification range. This extended solidification interval may promote elemental segregation, particularly of titanium and other γ′-forming elements, into the final solidifying regions of the melt pool. Such segregation can lead to the formation of brittle intermetallic phases such as η (Ni_3Ti), as discussed in the phase diagram analysis.

Together, the DSC and phase diagram analyses define the thermal processing window required to achieve a homogeneous, fully solutionized microstructure with desirable mechanical properties. This information is critical for optimizing LP-DED processing parameters and post-processing heat treatments to minimize segregation and eliminate deleterious secondary phases.

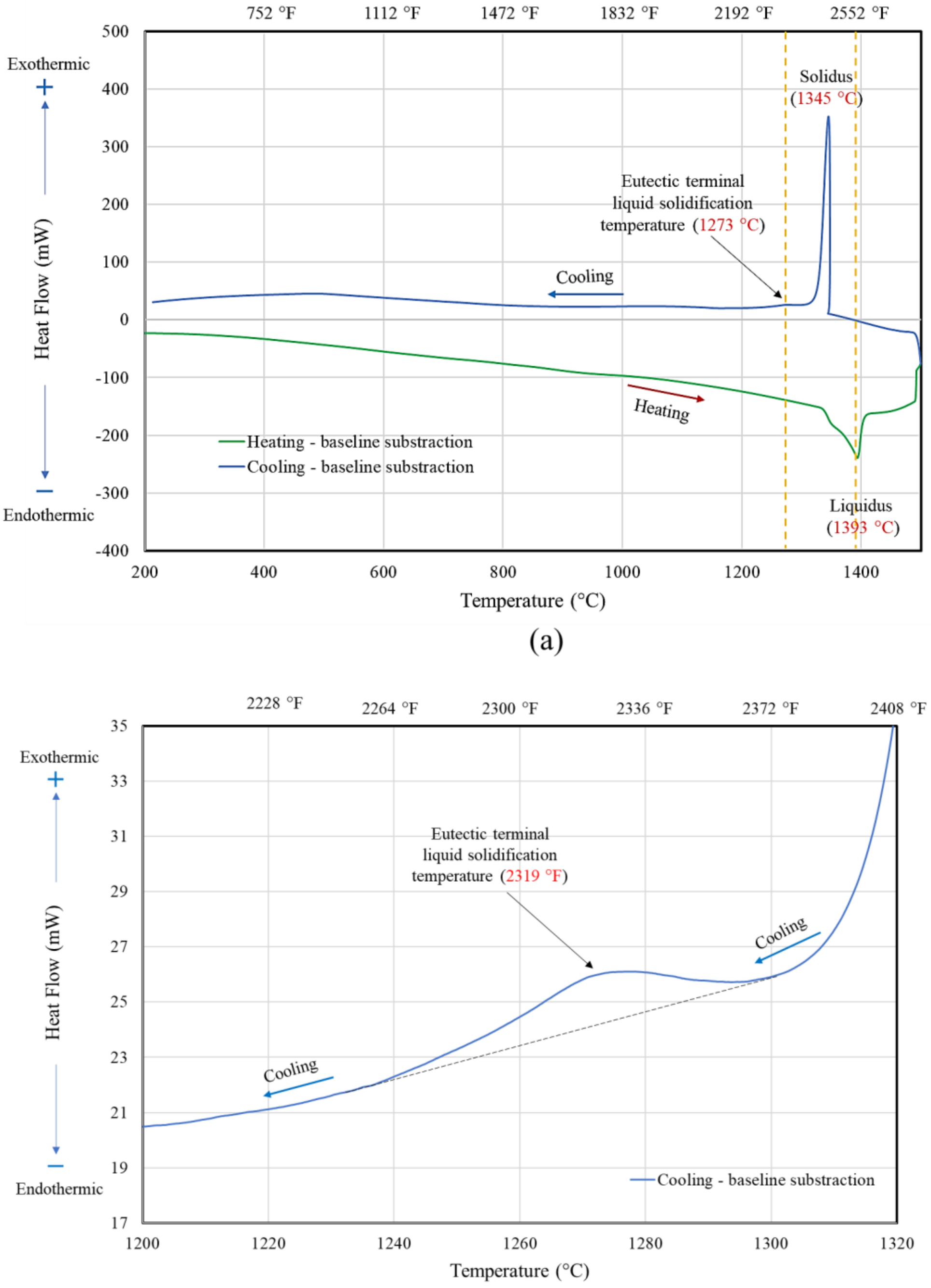

(a)

(b)

Figure 6. (a) DSC heating and cooling curves for as-built LP-DED NASA HR-1. (b) Close-up view of the terminal liquid solidification peak, which begins at approximately 2368 °F (1298 °C) and ends near 2260 °F (1238 °C).

Metal additive manufacturing processes such as LP-DED are fundamentally repeated welding operations, in which components are built layer-by-layer through localized melting of metal powder using a laser energy source. In many alloys, cracks can form during the terminal stages of solidification when liquid films persist along grain boundaries and, in some cases, interdendritic regions. At this stage, shrinkage strains across partially solidified boundaries can become significant, promoting solidification cracking.

For a given alloy system, the amount of terminal liquid is governed by the eutectic reaction occurring at the end of solidification. When sufficient terminal liquid is present, it can flow back into solidification cracks, providing a "crack-healing" effect that helps reduce or eliminate cracking. This mechanism is widely recognized as an important factor in mitigating solidification cracking[15].

Although metal AM processes typically produce much higher solidification cooling rates than conventional welding, the fundamental principles governingweldability and solidification cracking susceptibility remain applicable to AM materials. NASA HR-1 has demonstrated excellent printability when fabricated via LP-DED. This strong printability is attributed, at least in part, to the alloy's inherently low susceptibility to solidification cracking under the rapid solidification conditions of additive manufacturing.

3.3 Development of Aging Treatment

Aging treatment is performed after solution annealing treatment to precipitate and grow the strengthening γ' phase ($Ni_3(Ti,Al)$) [1]. During early development of LP-DED NASA HR-1, it was discovered that the standard single-step aging practice at 1325 °F (718.33 °C) for 16 hours did not adequately suppressthe precipitation of the brittle η-phase (Ni_3Ti) at grain boundaries, due to a high degree of Ti segregation arising from the LP-DED process. As a result, the aging temperature had to be lowered to mitigate η-phase formation. However, in LP-DED NASA HR-1, reducing the aging temperature to 1300 °F (704.44 °C) or 1275 °F (690.56 °C) results in a tensile strength reduction of approximately 5–15%.

To offset this strength loss while minimizing η-phase formation, the standard single-step aging treatment was modified into a two-step aging process. In γ'-strengthened superalloys, the first aging step at a higher temperature promotes the precipitation of secondary γ', while finer secondary or tertiary γ' precipitates from during the second step at a lower temperature[16–18]. This staged approach enhances precipitate number density and improves overall strengthening.

The hardness evolution after the first aging step at 1325 °F (718.33 °C), 1300 °F (704.44 °C), and 1275 °F (690.56 °C) is shown in Figure 7. For comparison, hardness values for wrought NASA HR-1 aged at 1325 °F (718.33 °C) and 1300 °F (704.44 °C) for 16 and 24 hours are also included. The results show that LP-DED HR-1 exhibits a more sluggish aging response than wrought HR-1.

Significant hardening occurs during aging, and longer soak times lead to progressive increases in hardness. The standard aging treatment at 1325 °F (718.33 °C) yields a hardness of 32.6 HRC after 16 hours. At 1300 °F (704.44 °C), the aging response is slower, with hardness reaching 28.5 HRC after 16 hours—approximately 4 points lower than at 1325 °F (718.33 °C). As expected, aging at 1275 °F (690.56 °C) results in the slowest hardening response.

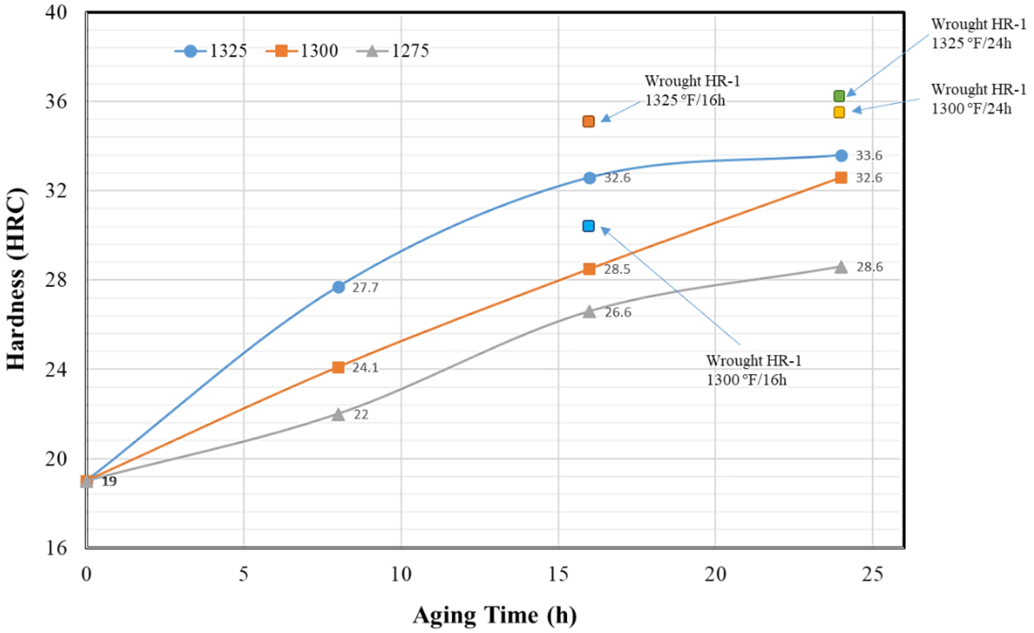

Figure 7. Hardness evolution of LP-DED NASA HR-1 after the first aging step at 1325 °F (718.33 °C), 1300 °F (704.44 °C), and 1275 °F (690.56 °C). Compared to wrought NASA HR-1, the LP-DED material exhibits a slower (more sluggish) aging response.

Microstructure evolution during aging at 1325 °F (718.33 °C), 1300 °F (704.44 °C), and 1275 °F (690.56 °C) is shown in Figure 8. As shown in Figure 8(a), grain boundaries are η-phase free after solution annealing treatment at 1800 °F for 1 hour. However, η-phase precipitation at grain boundaries is observed after aging at 1325 °F (718.33 °C) and 1300 °F (704.44 °C) for 24 hours (Figures 8(b) and 8(c)).

In contrast, aging at 1275 °F (691 °C) for 16 hours results in a significantly reduced volume fraction of grain-boundary η phase (Figure 8(d)), which remains minimal even after 24 hours. These observations indicate that lowering the first-step aging temperature effectively suppresses grain-boundary η-phase formation. Based on this microstructural assessment, 1275 °F (691 °C) for 16 hours was selected as the first-step aging condition.

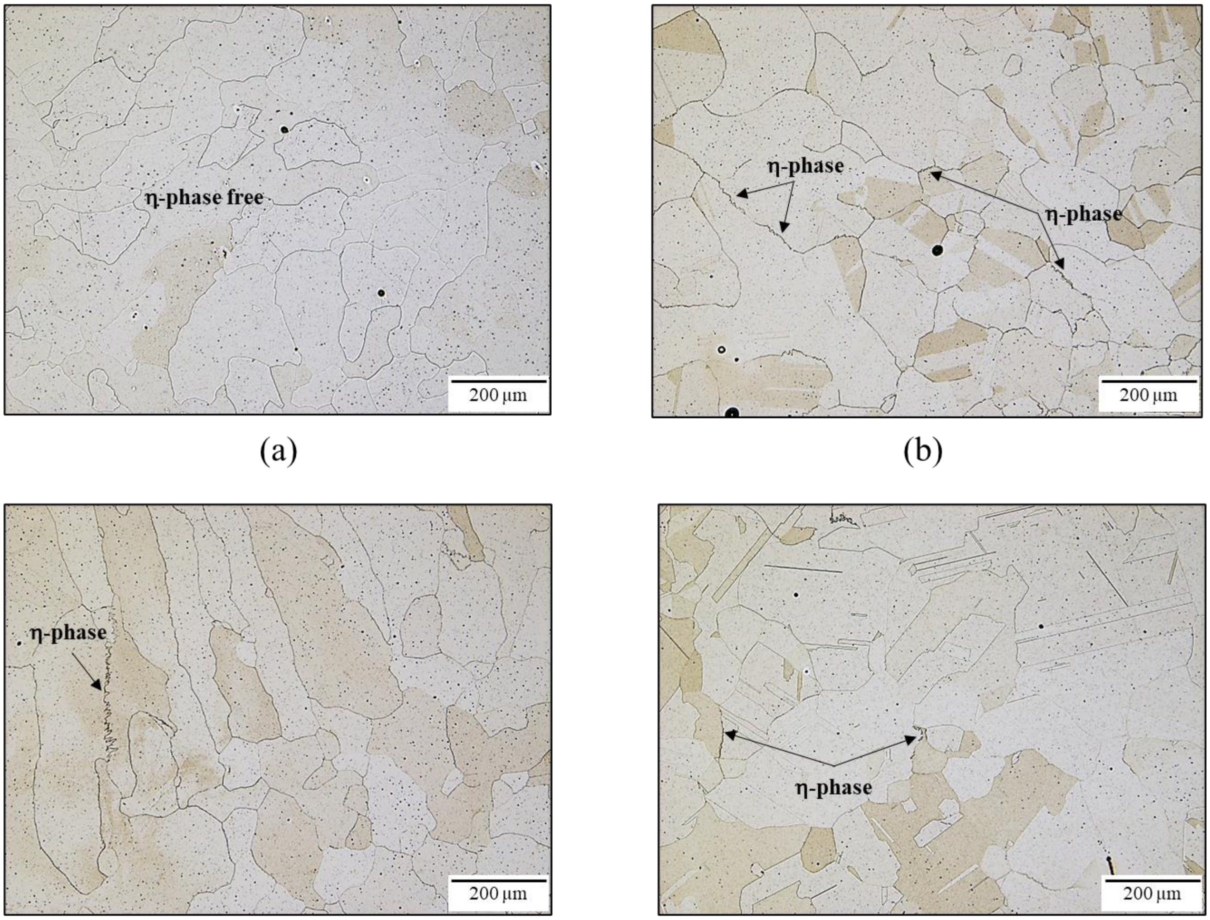

(a) (b)

(c) (d)

Figure 8. Grain-boundary η-phase precipitation after (a) solution annealing at 1800 °F for 1 h, (b) aging at 1325 °F (718.33 °C) for 24 h, (c) aging at 1300 °F (704.44 °C) for 24 h, and (d) aging at 1275 °F (690.56 °C) for 16 h. The volume fraction of grain-boundary η-phase is significantly reduced after aging at 1275 °F (690.56 °C) for 16 h.

A second-step aging was then subsequently performed at 1200 °F (648.89 °C) for 16 hours and 1150 °F (621.11 °C) for 16 hours to evaluate the effect of two-step aging on the hardening response. Figure 9 shows the hardness evolution after two-step aging at 1275 °F (690.56 °C)/16 h + 1200 °F (648.89 °C)/16 h and 1325 °F (718.33 °C)/16 h + 1150 °F (621.11 °C)/16 h. In both cases, the second aging step produces an additional hardness increase of approximately 5%, indicating further γ' precipitation and refinement.

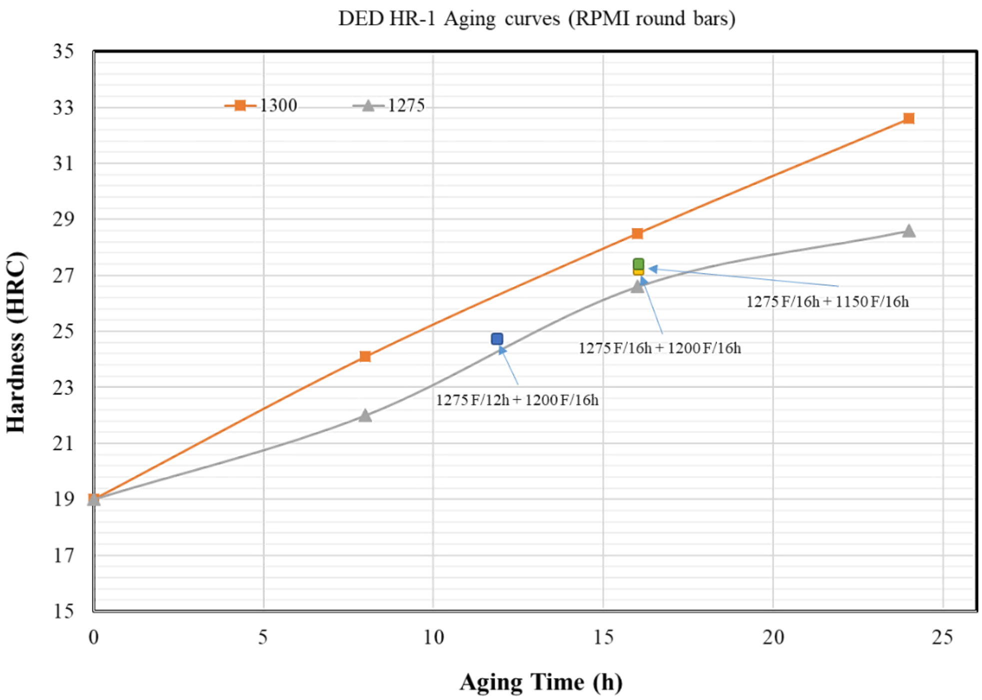

Figure 9. Effect of two-step aging on hardness evolution of LP-DED NASA HR-1.

Tensile tests were conducted in air at room temperature to evaluate the effects of aging treatments on the mechanical properties of LP-DED NASA HR-1. All specimens were machined from 0.6-inch diameter round bars (see Figure 2) . The tensile properties for the four aging conditions (A1–A4) are summarized in Table 2.

Compared to the standard single-step aging (A1), the two-step aging treatments (A3 and A4) produced slightly lower strength but significantly improved ductility and strain hardening capacity. These improvements are especially important for components such as liquid rocket engine (LRE) nozzles, where LCF is the primary life-limiting factor.

A1 (1325 °F [718.33 °C]/16 h) yielded the highest strength (YS: 109.60 ksi, UTS: 171.61 ksi) but also the lowest ductility (32.23%) and strain hardening exponent (n = 0.198), indicating a relatively less ductile response. In contrast, A4 (1275 °F [690.56 °C]/16 h + 1150 °F [621.11 °C]/16 h) showed the highest ductility (38.97%) and n value (0.271), though with the lowest yield strength (87.02 ksi). These improvements are attributed to refined γ′ precipitation and reduced grain-boundary η-phase formation. A3 (1275 °F [690.56 °C]/16 h + 1200 °F [648.89 °C]/16 h) provided a balanced combination of moderate strength and good ductility, while A2 (1300 °F [704.44 °C]/16 h) demonstrated a favorable trade-off between strength and ductility.

Overall, the results confirm that two-step aging treatments, particularly A4, substantially enhance ductility and strain hardening with an acceptable reduction in strength. Materials with higher n values can better store strain energy and increase resistance to LCF damage. Based on this performance, A4 has been selected as the preferred aging treatment for LP-DED NASA HR-1.

Table 2. Effect of one-step and two-step aging treatments on tensile properties of LP-DED NASA HR-1. The reported tensile properties for each aging condition represent the mean values obtained from eight independent samples.

Laser Power & Sample Configuration	Aging Treatment	Aging Treatment	Yield Stress (ksi)	Tensile Stress (ksi)	Fracture Elongation (%)	Strain hardening exponent (n)	n ranking
1070 W - round bar (0.6" diameter)	1325 °F (718.33 °C)/16h	A 1	109.60	171.61	32.23	0.198	4
	1300 °F (704.44 °C)/16h	A 2	88.44	162.74	37.87	0.263	2
	1275 °F (690.56 °C)/16h + 1200 °F (648.89 °C)/16h	A 3	92.95	166.19	36.74	0.251	3
	1275 °F (690.56 °C)/16h + 1150 °F (621.11 °C)/16h	A 4	87.02	162.40	38.97	0.271	1

3.4 Microstructure Evolution After Heat Treatment

Following fabrication by LP-DED, NASA HR-1 components require a sequence of post-processing heat treatmentsto transform the as-fabricated part into a functional, end-use component. The standard heat treatment sequence for LP-DED NASA HR-1 is provided in Table 3.

These post-processing heat treatments drive progressive microstructural evolution through mechanisms including recovery, recrystallization, grain growth, and precipitation of strengthening phases. To study the evolution of microstructure after each step, a series of heat treatment conditions—designated HT-A (as-built) through HT-G (two-step aged)—were applied to LP-DED NASA HR-1 samples. This structured approach enables direct assessment of microstructural development at each stage of processing.

Table 3. Summary of the post-processing heat treatment steps applied to investigate microstructure evolution in LP-DED NASA HR-1.

Heat Treatment		Heat Treatment Steps				
HT-A	As-built	-	-	-	-	-
HT-B	Stress-relief	1950 °F (1065.56 °C) /1.5h	-	-	-	-
HT-C	Homogenization	1950 °F (1065.56 °C)/1.5h	2125 °F (1162.78 °C)/6h	-	-	-
HT-D	Solution anneal	1950 °F (1065.56 °C)/1.5h	2125 °F (1162.78 °C)/6h	1950 °F (1065.56 °C)/1h	-	-
HT-E	1-step age	1950 °F (1065.56 °C)/1.5h	2125 °F (1162.78 °C)/6h	1950 °F (1065.56 °C)/1h	1325 °F (718.33 °C)/16h	-
HT-F	2-step age, step 1	1950 °F (1065.56 °C)/1.5h	2125 °F (1162.78 °C)/6h	1950 °F (1065.56 °C)/1h	1275 °F (690.56 °C)/16h	-
HT-G	2-step age, both steps	1950 °F (1065.56 °C)/1.5h	2125 °F (1162.78 °C)/6h	1950 °F (1065.56 °C)/1h	1275 °F (690.56 °C)/16h	1150 °F (621.11 °C)/16h

3.4.1 HT-A: As-Built

The as-built microstructure of LP-DED NASA HR-1 is shown in the optical micrographs in Figure 10. In the XZ orientation (parallel to the build direction), the microstructure exhibits arc-shaped boundaries and overlapping melt pools resulting from the layer-by-layer deposition process, as shown in Figure 10(a). The melt pool width ranges from approximately 1.5 to 1.7 mm. Figure 10(b) shows the XY cross section (perpendicular to the build direction), where cross hatches within a single layer are visible as diagonal patterns across the micrograph, reflecting the scan strategy employed during deposition.

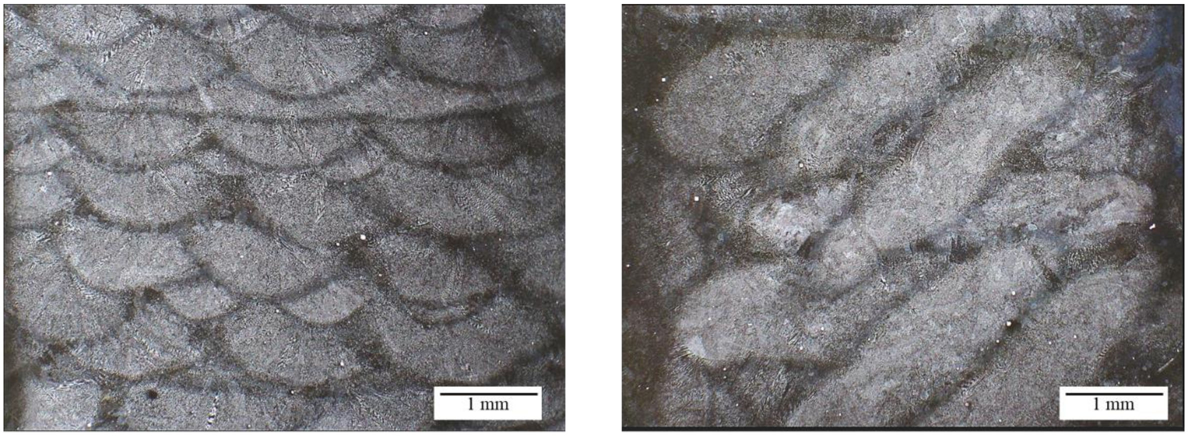

(a) (b)

Figure 10. Optical micrographs of as-built LP-DED NASA HR-1 showing microstructure in (a) XZ orientation and (b) XY orientation.

Figure 11 shows the typical melt pool structure and epitaxial dendrite formation in LP-DED NASA HR-1, observed using both dark-field and bright-field imaging modes. Both images were taken from the XZ orientation. Epitaxial dendrite growth through multiple melt pools is visible in Figure 11(a), indicated by the white arrow. This columnar grain structure develops as a result of the high solidification rate and steep thermal gradients is a dominant feature in microstructure evolution, typically aligned with the thermal gradient direction[19].

Fine dendritic structures, including growth through the melt pool boundaries, are clearly observed in the bright-field image (Figure 11(b)). The orange dotted line marks the boundary between successive melt pool layers in the build direction, while the black dotted arrows indicate the primary dendrite growth directions.

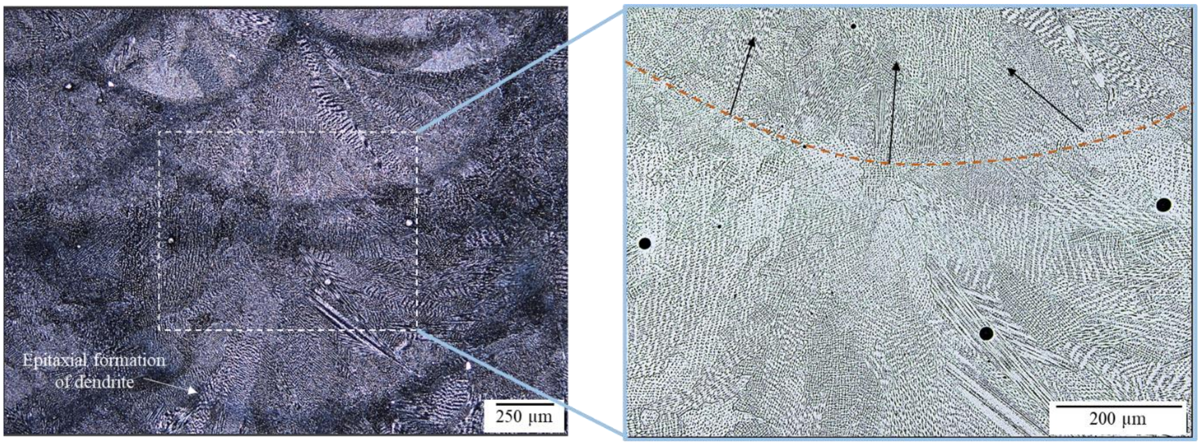

(a) (b)

Figure 11. (a) Dark-field image of as-built LP-DED NASA HR-1 showing melt pool boundaries and epitaxial dendrite growth. (b) Bright-field image showing dendritic microstructure and the directions of dendrite growth (indicated by black arrows) within the highlighted region (white box) in (a).

SEM backscatter images further highlight the melt pool morphology and epitaxial dendrite grain structure of LP-DED NASA HR-1, as shown in Figure 12. Numerous small grains are visible in Figure 12(a), while Figure 12(b) highlights the dendrite growth directions (indicated by red arrows), which vary due to complex heat dissipation and thermal gradients during cooling [20].

The DSC curve showing phase transformations during heating of as-built LP-DED NASA HR-1 is presented in Figure 13. The as-built condition (HT-A) exhibits a notable change in heat flow between 870 °C (1598 °F) and 1010 °C (1850 °F), corresponding to dissolution of γ′ ($Ni_3(Al,Ti)$) into the γ matrix[21]. This behavior indicates that γ′ precipitates during the LP-DED process as a result of intrinsic thermal cycling and non-equilibrium solidification.

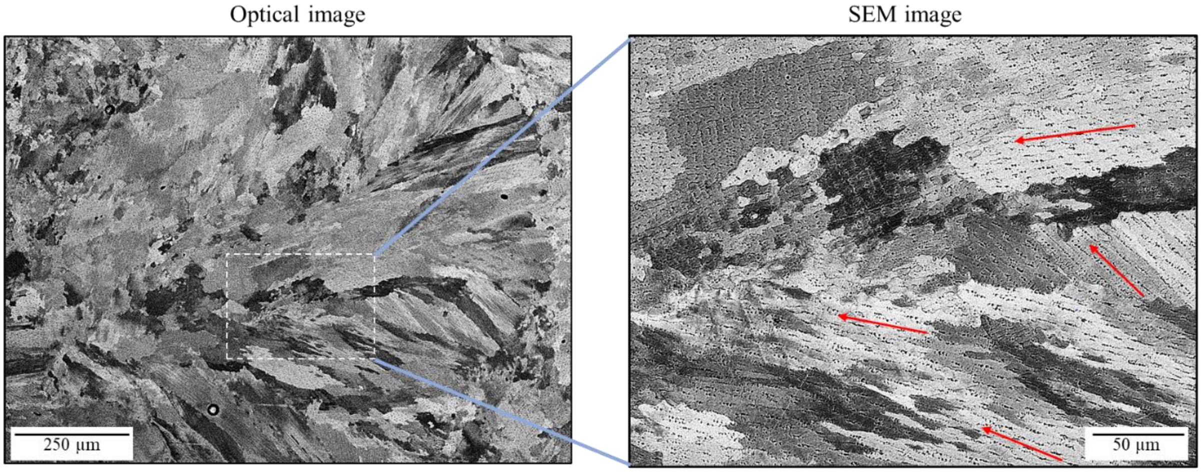

(a) (b)

Figure 12. SEM backscatter images showing (a) the as-built melt pool and grain structures, and (b) the dendritic structure and dendrite growth directions (indicated by red arrows) within the highlighted region (white box) in (a).

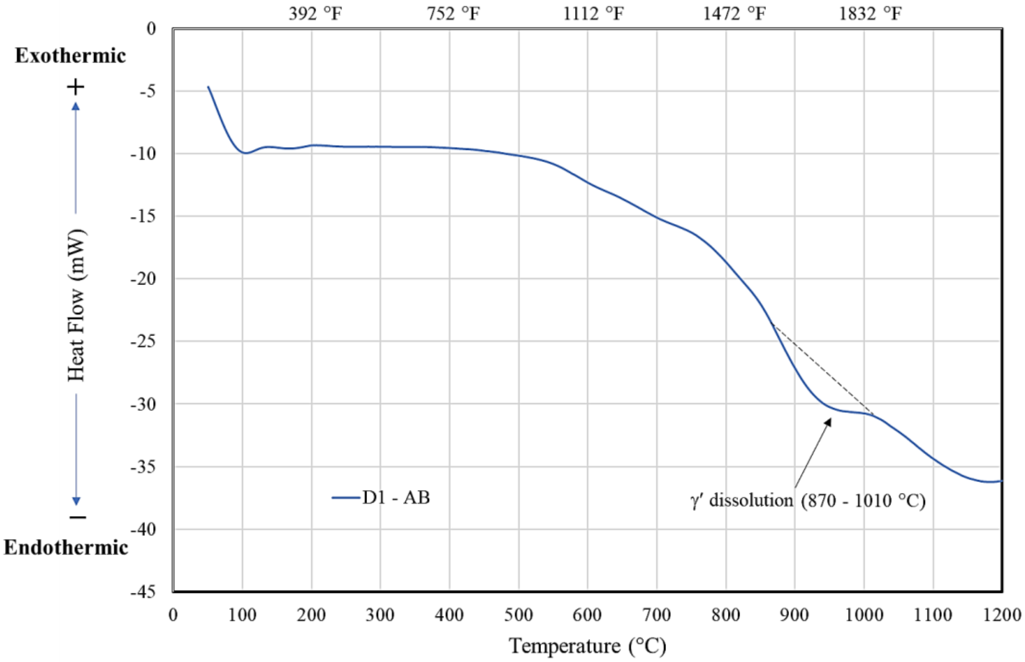

Figure 13. DSC heating curve of as-built LP-DED NASA HR-1. A distinct endothermic γ′ dissolution peak begins near 1598 °F (870 °C) and completes around 1850 °F (1010 °C).

3.4.2 HT-B: Stress Relief

Stress relief treatment can lead to recovery, recrystallization, and grain growth, depending on the applied temperature and hold time. Figure 14 illustrates the microstructural evolution in both the XZ and XY orientations following stress relief at 1950 °F (1065.56 °C) for 1.5 hours. As shown, partial recrystallization occurred during stress relief, and the melt pool structure and hatch pattern observed in the as-built specimens are no longer evident. The driving force for recrystallization is attributed to the high residual stresses and plastic strain accumulated during the repeated thermal cycling inherent to the LP-DED process[22-24].

The resulting microstructure consists of a mixture of recovered (unrecrystallized) and recrystallized grains, as illustrated in Figure 14. Some remnants of the original dendritic structure are still visible. After the stress relief cycle, the samples were furnace-cooled to 1200 °F (648.89 °C) at a very slow rate to minimize thermal distortion. As a result of the slow cooling, precipitation of the undesirable brittle η-phase (Ni_3Ti) occurred along select grain boundaries (Figure 15(a)). Numerous annealing twins were also observed after stress relief at 1950 °F (1065.56 °C), as shown in Figure 15(b), consistent with recrystallization in a FCC superalloy system.

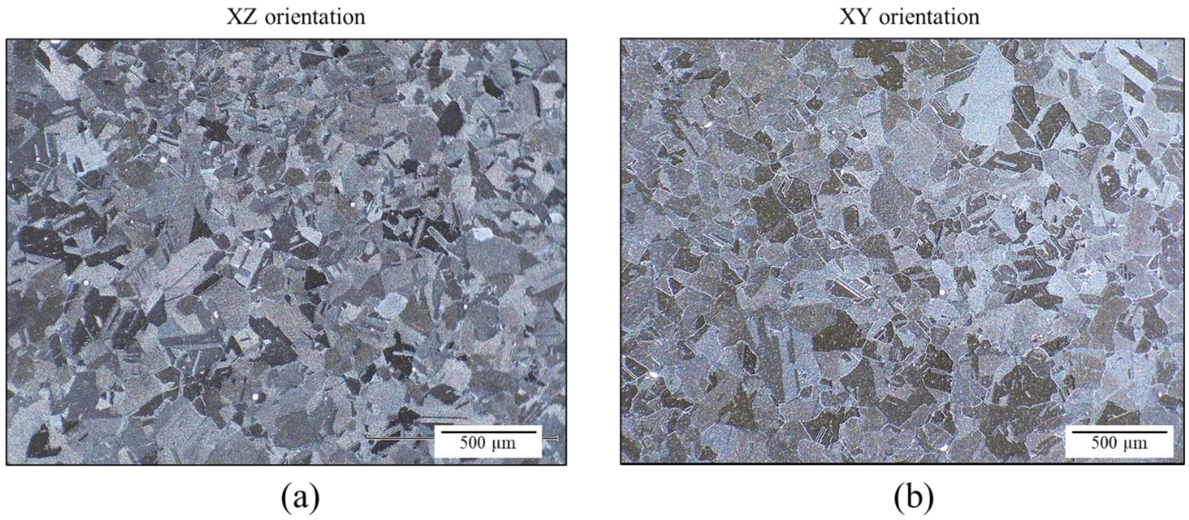

Figure 14. Optical micrographs showing the microstructure evolution of LP-DED NASA HR-1 after stress relief at 1950 °F (1065.56 °C) for 1.5 hours: (a) XZ orientation and (b) XY orientation.

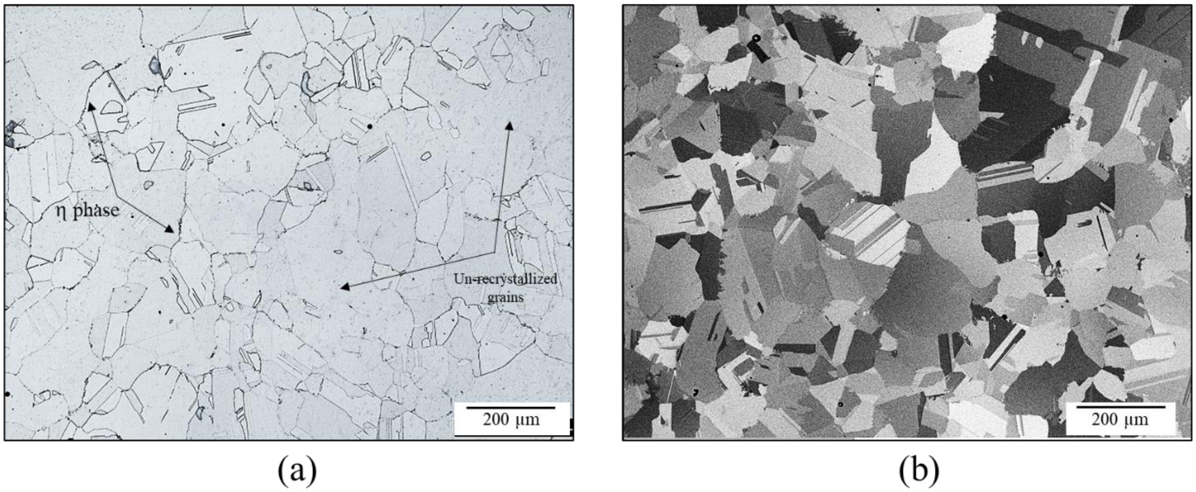

Figure 15. (a) Microstructure of LP-DED NASA HR-1 after stress relief, showing a mixture of recovered (unrecrystallized) and recrystallized grains. Occasional precipitation of the brittle η-phase (Ni_3Ti) is observed along grain boundaries. (b) Backscattered SEM image of the same condition, highlighting recrystallized and recovered grains with numerous annealing twins.

Figure 16 shows the phase transformations observed during heating to 2192 °F (1200 °C) for stress-relieved LP-DED NASA HR-1. The DSC heating curves for the as-built (HT-A) and stress-relieved (HT-B) conditions are superimposed to compare the microstructural evolution before and after stress relief. As shown, the stress-relieved material exhibits a clear exothermic reaction between 1150 °F (621.11 °C) and 1438 °F (781 °C), corresponding to γ' precipitation during heating. This is followed by a distinct endothermic reaction between 1553 °F (845 °C) and 1729 °F (943 °C), associated with γ' dissolution into the γ matrix.

The increased magnitude of the γ′ dissolution peak after stress relief indicates a higher volume fraction of γ′, likely resulting from slow furnace cooling following the 1950 °F (1065.56 °C) stress relief treatment. Although η was observed at grain boundaries by optical microscopy after stress relief at 1950 °F (1065.56 °C), no distinct η-dissolution peak appeared in the DSC heating curve, likely because η was confined to localized grain boundaries with a volume fraction that falls below the detection sensitivity of DSC.

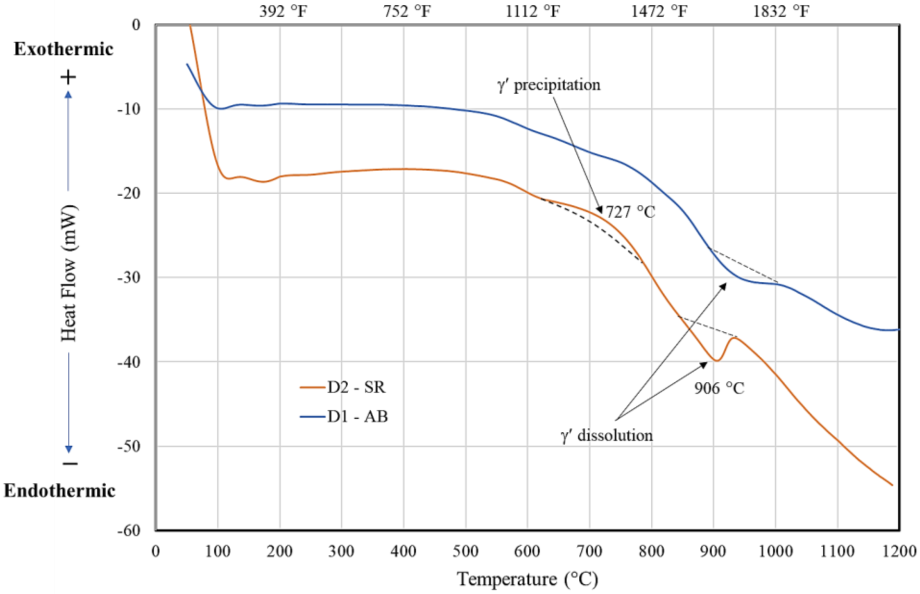

Figure 16. DSC heating curves for as-built and stress-relieved LP-DED NASA HR-1. The curve for the as-built condition (HT-A) is superimposed for comparison. The stress-relieved sample exhibits an exothermic γ′ precipitation peak at 1341 °F (727 °C), followed by a γ′ dissolution endotherm between 1553–1729 °F (845–943 °C).

3.4.3 HT-C: Homogenization

A significant microstructural transformation occurs after homogenization. The evolution of the microstructure after homogenization at 2125 °F (1162.78 °C) for 6 hours, followed by argon quench cooling, is shown in Figure 17. Although the homogenized microstructure appears similar to the stress-relieved condition (compare Figures 14 and 17), close examination using multiple imaging modes reveals that the degree of recrystallization increases substantially after homogenization, as shown in Figure 18. The homogenized microstructure consists of fully recrystallized, equiaxed grains, and the grain boundaries appear η-phase free (Figure 18(a)). This can be attributed to the rapid cooling rate associated with the argon quench, which suppresses precipitation of the brittle η-phase. Numerous annealing twins also formed during homogenization, as shown in Figure 18(b). Overall, the homogenization treatment promotes a higher degree of recrystallization and produces a more uniform microstructure in LP-DED NASA HR-1.

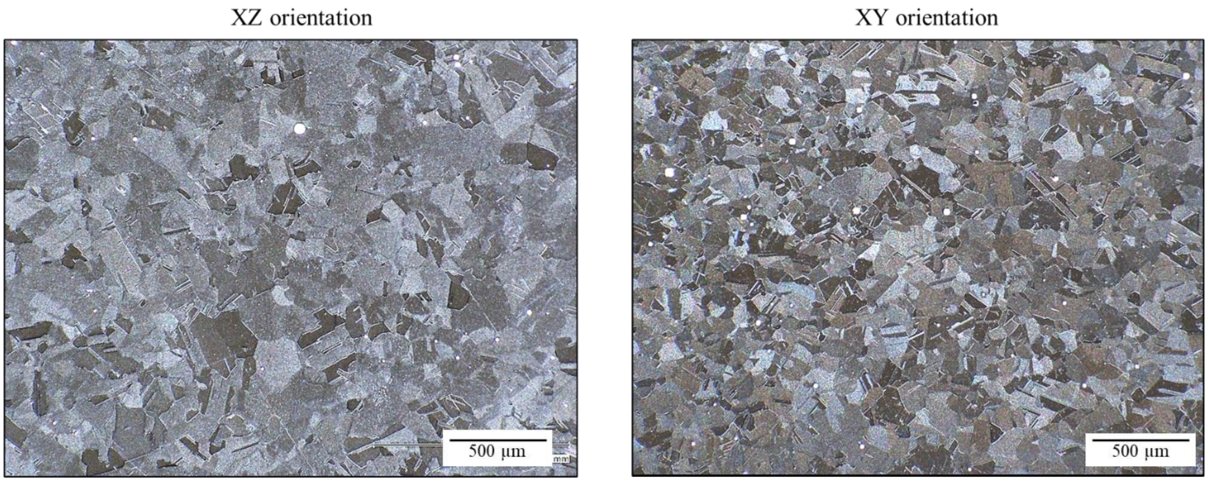

(a) (b)

Figure 17. Optical micrographs showing the microstructure of LP-DED NASA HR-1 after homogenization at 2125 °F (1162.78 °C) for 6 hours followed by argon quenching, in (a) XZ and (b) XY orientations.

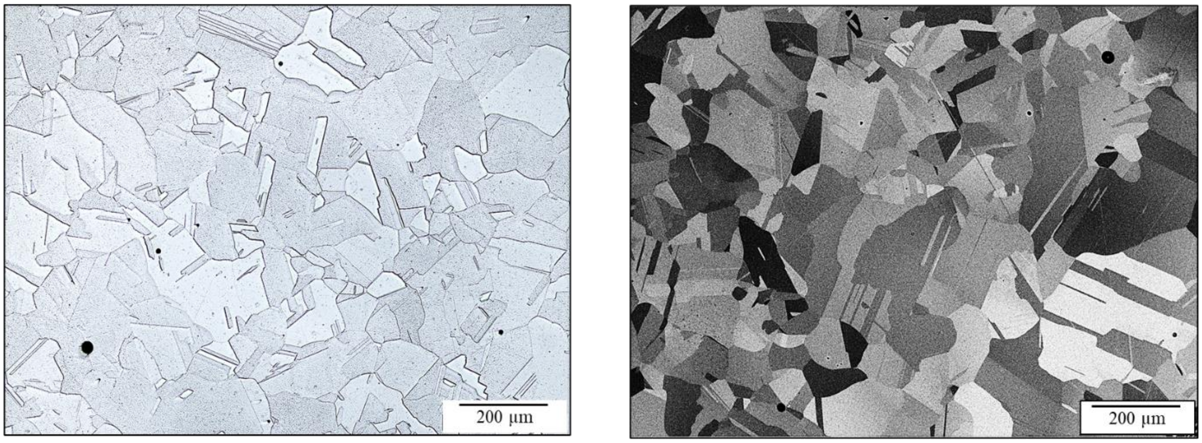

Figure 18. (a) The microstructure is fully recrystallized, with no detectable brittle η-phase (Ni_3Ti) at grain boundaries following homogenization. (b) SEM backscattered electron image showing numerous annealing twins in the fully recrystallized microstructure.

The DSC curve for the homogenized condition is shown in Figure 19. The heating curves of the as-built and stress-relieved samples are superimposed to compare microstructural evolution after stress relief and homogenization. As shown, the homogenized sample exhibits a distinct exothermic peak starting at 1202 °F (650 °C) and ending at 1428.8 °F (776 °C), corresponding to the precipitation of γ' during heating. A similar change in heat flow is also observed in the stress-relieved sample. However, the magnitude of the heat flow change is more pronounced (i.e., a larger peak) in the homogenized sample. The presence of a more pronounced γ' precipitation peak can be attributed to the greater volume fraction of γ' formed during homogenization.

This enhanced γ′ precipitation is due to increased availability of Ti and Al in the γ matrix (Fe-Ni-based solid solution) following homogenization. Similar to the stress-relieved sample, a distinct endothermic peak appears at approximately 1653.8 °F (901 °C) (starting at 1553 °F [845 °C] and ending at 1707.8 °F [931 °C]), corresponding to the dissolution of γ′ into the γ matrix.

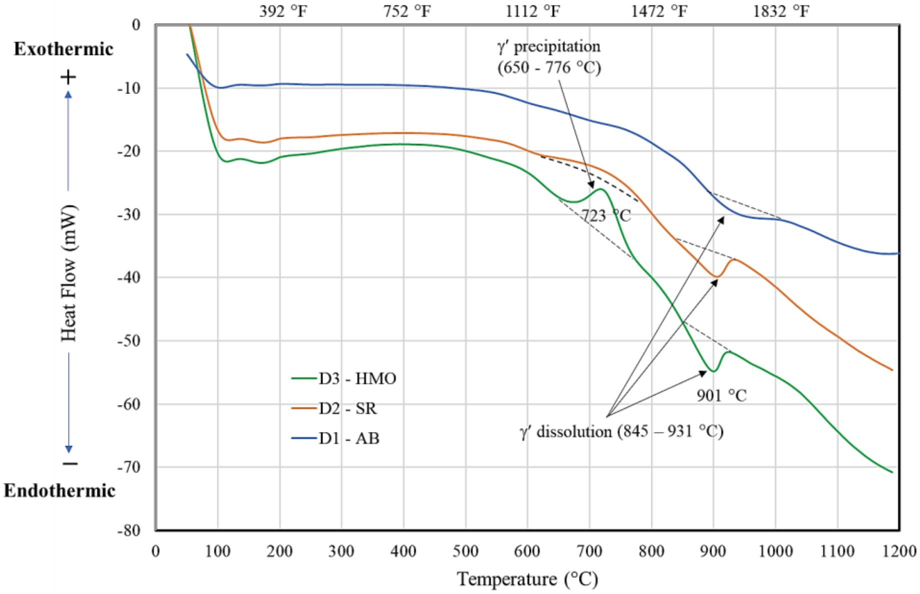

Figure 19. DSC heating curves for as-built and homogenized LP-DED NASA HR-1. The homogenized sample shows a distinct exothermic peak from 1202 °F (650 °C) to 1428.8 °F (776 °C), corresponding to γ′ precipitation. A pronounced endothermic γ′ dissolution peak begins at approximately 1553 °F (845 °C) and ends near 1708 °F (931 °C).

3.4.4 3D Microscopy

Figure 20 presents 3D microscopy images showing the microstructural evolution from the as-built condition through homogenization treatment (HT-C), viewed in all three orientations (XZ, YZ, and XY). In the as-built condition (HT-A), layer boundaries and melt pool traces are the dominant features, as shown in Figure 20(a), reflecting the layer-by-layer deposition process inherent to LP-DED. Post-processing heat treatments introduced significant microstructural changes, as the applied thermal energy drives recovery and recrystallization.

Although the 3D microstructures of the stress-relieved (HT-B) and homogenized (HT-C) samples appear similar at low magnification, the homogenization treatment results in a higher degree of recrystallization and more well-defined grain boundaries. As illustrated in Figure 20(b), some regions in the HT-B condition remain only partially recrystallized. In contrast, the HT-C condition shows more complete recrystallization, with a uniform grain structure across all three orientations. These observations confirm that homogenization promotes a higher degree of microstructural uniformity compared to stress relief alone.

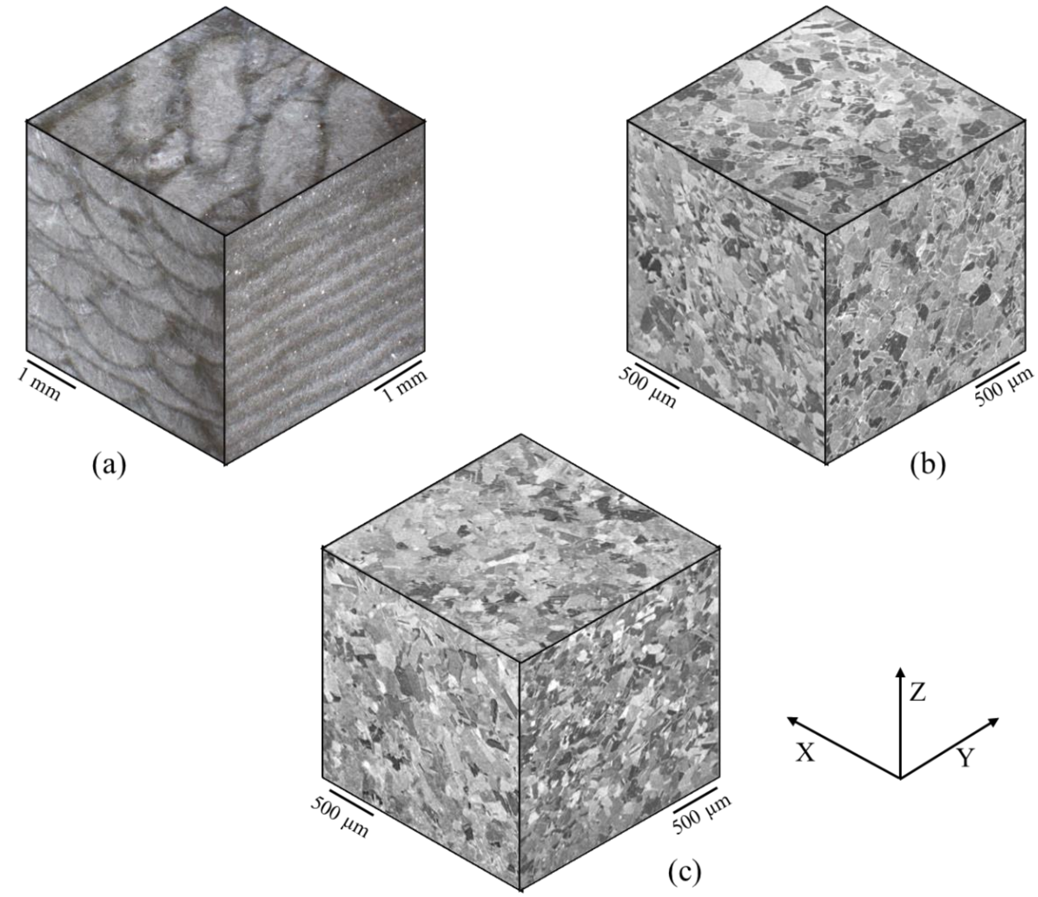

Figure 20. 3D metallography showing the front (XZ), side (YZ), and top (XY) views of the microstructure in LP-DED NASA HR-1 samples: (a) as-built condition, (b) after stress relief, and (c) after homogenization treatment.

3.4.5 HT-D: Solution Annealing Treatment

After homogenization, solution annealing and aging treatments are performed sequentially. The solution anneal was conducted above the η-phase solvus temperature to dissolve any undesirable η-phase that may have formed during cooling from the homogenization step. In contrast to homogenization, the subsequent solution annealing treatment does not appear to produce additional recrystallization or noticeable grain growth. The grain structure remains fully recrystallized and stable, indicating that the primary microstructural framework was established during homogenization.

The DSC heating curves of the homogenized and solution annealed samples are superimposed in Figure 21 to compare their thermal behavior. As shown, both curves exhibit a pronounced γ′ precipitation peak at approximately 1333 °F (723 °C), followed by a γ′ dissolution peak near 1654 °F (901 °C). The similarity of these thermal responses indicates that the overall precipitation behavior of γ′ remains largely unchanged by the solution annealing step.

For LP-DED NASA HR-1, homogenization primarily serves to reduce elemental segregation resulting from solidification. In contrast, the main objective of the solution annealing treatment is to ensure that any residual η-phase formed during cooling after homogenization is fully dissolved into the γ solid solution. Therefore, it is not surprising that the DSC heating curves look similar before and after solution annealing treatment.

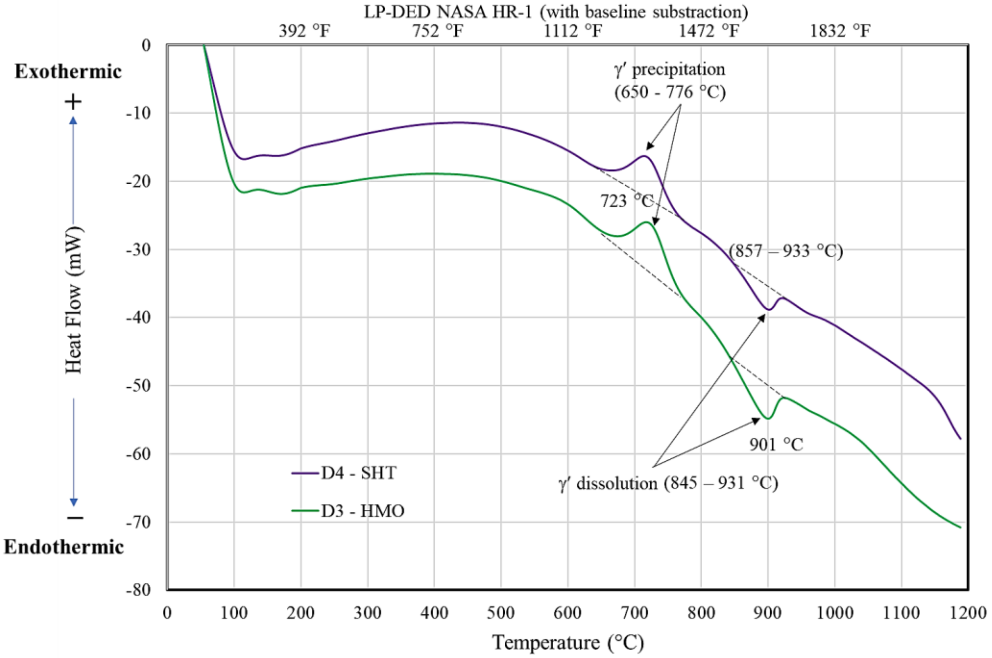

Figure 21. DSC heating curve for solution annealed LP-DED NASA HR-1, with the curve for the homogenized condition superimposed for comparison. Both conditions exhibit a distinct exothermic γ′ precipitation peak near 1333 °F (723 °C), followed by an endothermic γ′ dissolution peak around 1654 °F (901 °C), showing similar thermal behavior.

3.4.6 HT-E: One-Step Aging Treatment

Figure 22 shows the DSC heating curve after the one-step aged condition (HT-E). The heating curves for the as-built (HT-A) and solution annealed (HT-D) samples are superimposed to compare the microstructural evolution from the as-built to fully heat-treated condition. As shown, the DSC curves for both the solution annealed and one-step aged samples exhibit a pronounced γ′ precipitation peak between 1324 and 1337 °F (718 °C–725 °C), followed by a γ′ dissolution peak at approximately 1652 °F (900 °C).

The γ′ dissolution peak is noticeably larger (in peak area) in the one-step aged sample than the solution annealed sample. This indicates a greater volume fraction of γ′ precipitates formed during the aging process. Following γ′ dissolution, a gradual change in heat flow is observed between 1834 °F (1001 °C) and 1976 °F (1080 °C). This thermal event is attributed to η-phase precipitation. Previous studies have reported γ′→η transformation can occur under overaged conditions, such as in superalloy A-286 [25]. Additionally, η-phase formation has been reported in γ′-strengthened AM Ni-based superalloys at around 1160 °C, close to the η-phase precipitation peak observed in Figure 22 [26]. Therefore, the η-phase formation detected during DSC heating likely results from γ′ overaging in the one-step aged condition.

Figure 23 shows the microstructure of LP-DED NASA HR-1 after one-step aging. The structure consists of fully recrystallized grains with numerous annealing twins. Notably, the brittle η-phase (Ni_3Ti) was not detected at grain boundaries in this condition by optical or SEM examination.

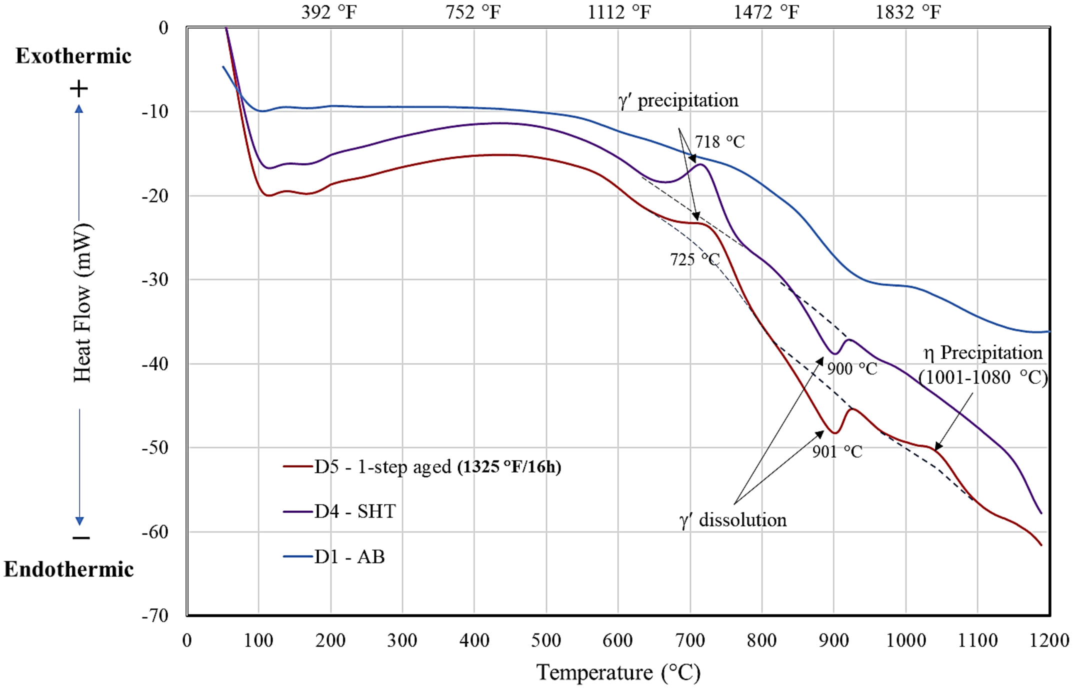

Figure 22. DSC heating curves showing the evolution of γ′ precipitates after one-step aging treatment (HT-E). The DSC curves of as-built and solution annealed LP-DED NASA HR-1 are superimposed for comparison. Both one-step aged and solution-treated conditions exhibit a distinct exothermic γ′ precipitation peak near 1333 °F (723 °C), followed by an endothermic γ′ dissolution peak around 1654 °F (901 °C), and an exothermic η-phase precipitation between 1834 °F (1001 °C) and 1976 °F (1080 °C).

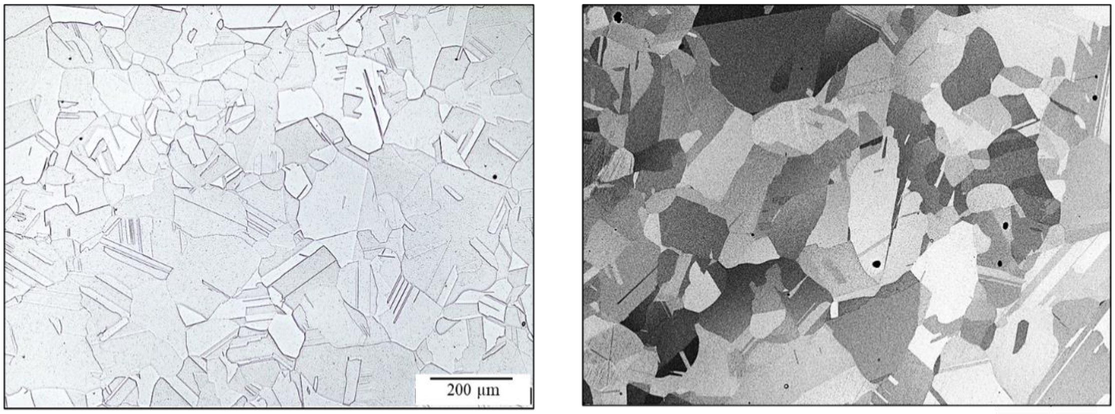

(a) (b)

Figure 23. (a) Grain boundaries appear clean, with no detectable brittle η-phase (Ni_3Ti). (b) SEM backscattered image showing a fully recrystallized microstructure with numerous annealing twins after the one-step aging treatment.

3.4.7 HT-F and HT-G: Two-Step Aging Treatment

The effects of the first and second aging steps (HT-F and HT-G) on phase transformations are shown in Figure 24. As illustrated, the DSC heating curves for HT-F and HT-G samples appear similar, both featuring a small exothermic γ′ precipitation peak, followed by an endothermic γ′ coarsening peak between approximately 1337–1553 °F (725–845 °C), and a γ′ dissolution peak between 1571–1715 °F (855–935 °C).

However, there are noticeable differences in the size and shape of the γ′ coarsening and dissolution peaks before and after the second aging step at 1150 °F (621.11 °C) for 16 hours. The γ′ coarsening peak in the two-step aged sample (HT-G) is slightly broader and more pronounced than that of the single-step aged sample (HT-F, aged only at 1275 °F (690.56 °C) for 16 hours). This behavior suggests the presence of a greater volume fraction of fine, underaged γ′ precipitates in the HT-G sample, which coarsen more readily during DSC heating.

Additionally, the γ′ dissolution peak is significantly larger in the HT-G sample compared to HT-F, indicating an increased γ′ volume fraction after completion of the second aging step. These observations confirm that the second aging treatment enhances precipitation strengthening.

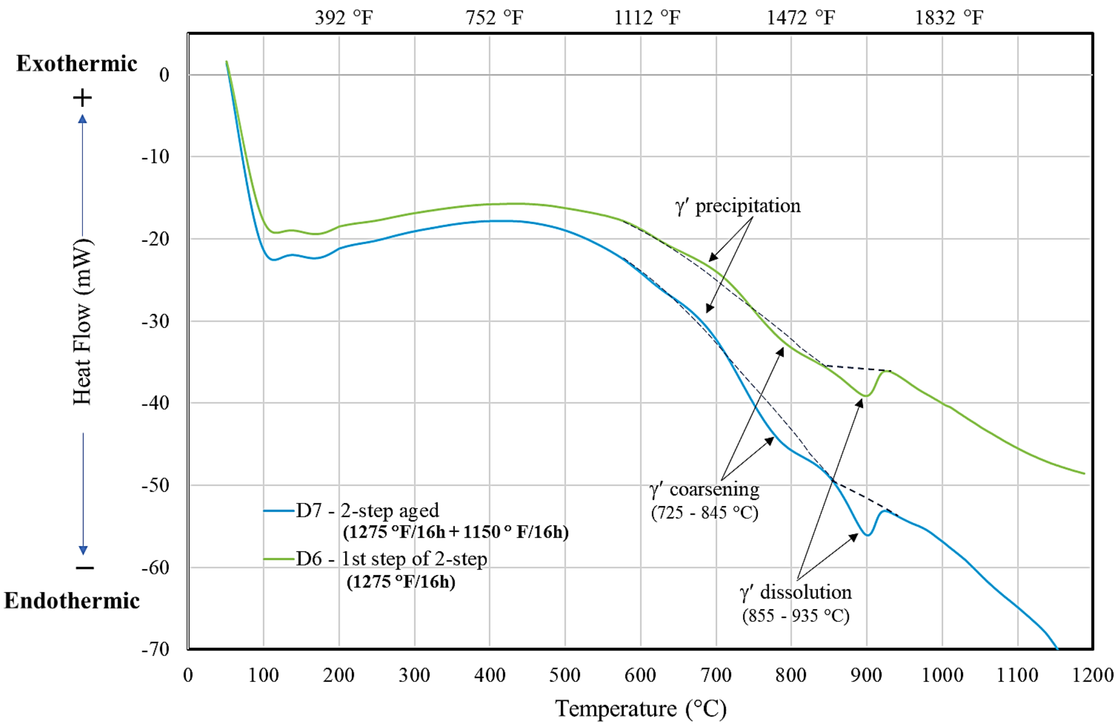

Figure 24. DSC heating curves showing the evolution of γ′ precipitation for samples aged under HT-F (1275 °F (690.56 °C)/16 h) and HT-G (1275 °F (690.56 °C)/16 h + 1150 °F (621.11 °C)/16 h) conditions. Both display a small exothermic γ′ precipitation peak, followed by an endothermic γ′ coarsening peak between approximately 1337–1553 °F (725–845 °C), and a γ′ dissolution peak between 1571–1715 °F (855–935 °C).

Figure 25 compares the DSC heating curves for the one-step (HT-E) and two-step (HT-G) aged conditions. The most notable differences between the curves are the absence of a well-defined γ′ precipitation peak and the presence of a distinct γ′ coarsening peak in the two-step aged sample (HT-G). It has been reported that aging at lower temperatures increases the volume fraction of γ′ precipitate and refines its size in Ni-based superalloys such as X-750 [27]. Therefore, the absence of a γ′ precipitation peak in the two-step aged sample likely reflects the reduced driving force for additional γ′ formation during DSC heating, as a substantial fraction of γ′ has already precipitated during the second aging step.

The two-step aged sample also exhibits a larger γ′ coarsening peak, suggesting that the γ′ particles were significantly finer prior to DSC testing compared to those in the one-step aged condition. This is consistent with literature showing that lower aging temperatures promote the formation of finer, more numerous γ′ particles[27]. As a result, significant γ′ particle growth and coalescence occurred in the two-step aged sample during DSC heating.

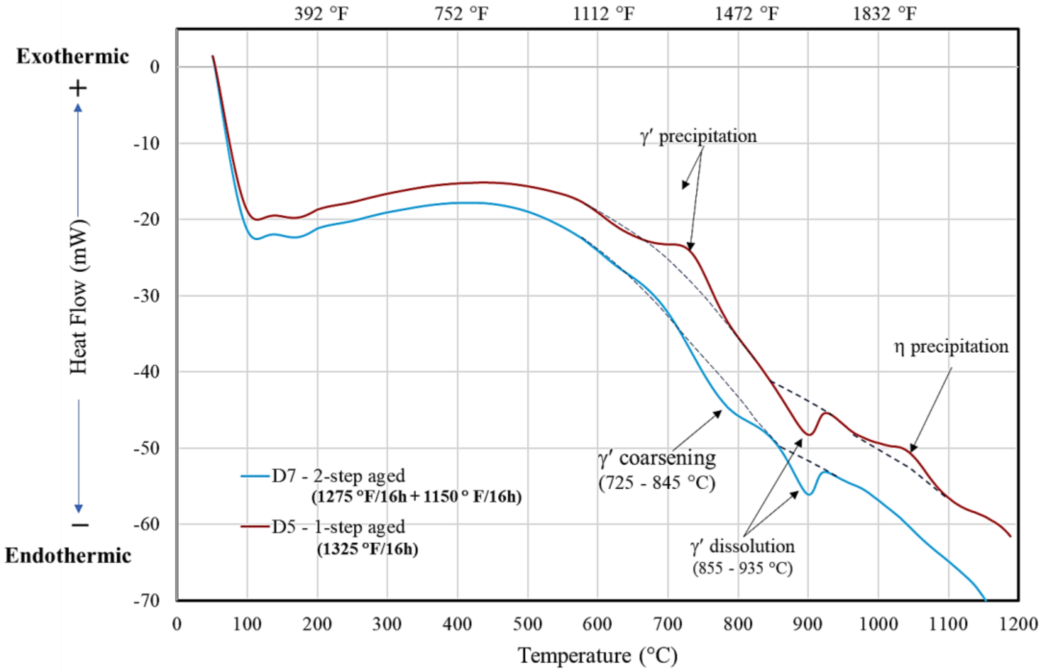

Figure 25. DSC heating curves showing the evolution of γ′ precipitation behavior before and after one-step and two-step aging treatments. The most notable differences are the absence of a well-defined γ′ precipitation peak and the presence of a distinct γ′ coarsening peak in the two-step aged material (HT-G), likely due to a higher volume fraction of γ′ formed during the second aging step.

A fundamental distinction between the one-step and two-step aged conditions is the emergence of an η-phase precipitation peak in the one-step aged material following γ′ dissolution, whereas no such peak is observed in the two-step aged sample during DSC heating. This difference indicates that the two-step aging treatment significantly reduces susceptibility to the γ′ → η transformation and enhances phase stability during thermal exposure.

The improved stability arises from differences in precipitate distribution and solute partitioning. In the one-step aged condition, the higher aging temperature promotes Ti segregation to grain boundaries. Upon DSC heating, dissolution of γ′ between approximately 1571–1715 °F (855–935 °C)locally enriches the surrounding matrix in Ti, generating supersaturation at grain boundaries and providing a strong thermodynamic driving force for η nucleation. This process produces the distinct exothermic peak near 1886 °F (1030 °C).

In contrast, the two-step aging treatment produces a finer, more uniform γ′ distribution and reduces grain-boundary Ti enrichment. The lower second-step aging temperature limits solute redistribution and delays precipitate coarsening, thereby minimizing local Ti supersaturation during γ′ dissolution. As a result, η nucleation is effectively suppressed. Notably, the grain structure remains unchanged between the two conditions, confirming that the observed differences arise from precipitate evolution rather than recrystallization or grain growth.

Mechanically, the two-step aged material exhibits higher tensile ductility and a greater strain hardening exponent than the one-step aged condition[6]. A higher strain hardening exponent promotes more uniform plastic deformation, increases strain energy absorption, and improves resistance to LCF. Collectively, these results demonstrate that two-step aging enhances both microstructural stability and mechanical performance, making it the preferred treatment for LP-DED NASA HR-1 components subjected to cyclic loading in hydrogen-rich environments.

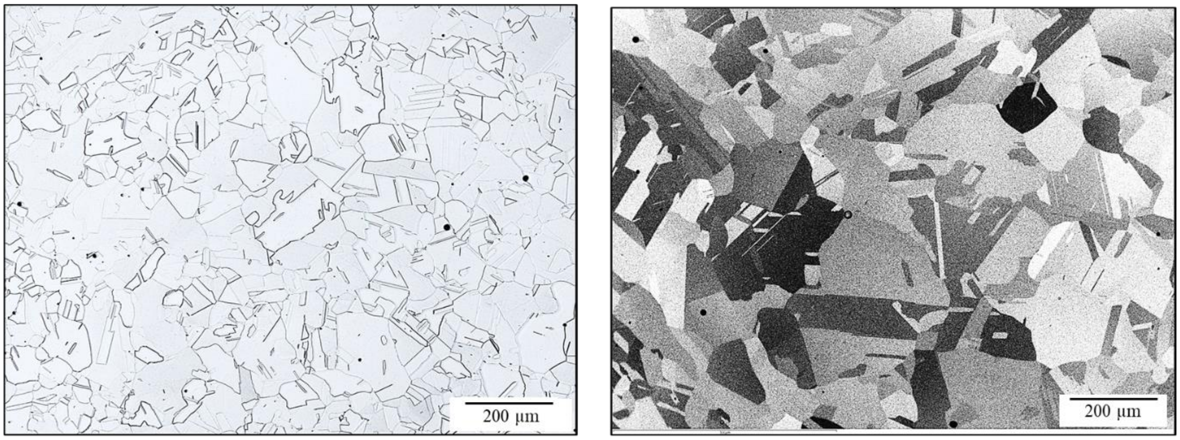

(a) (b)

Figure 26. (a) After two-step aging, the microstructure appears clean with no detectable brittle η-phase (Ni_3Ti) at grain boundaries. (b) SEM backscattered image showing fully recrystallized grains containing numerous annealing twins following the two-step aging treatment.

3.5 γ′ In Laser Powder Directed Energy Deposition (LP-DED) NASA HR-1

The exceptional high-temperature performance of Fe-Ni-based superalloys can be attributed to their complex microstructure—most notably the precipitation of the γ′ phase ($Ni_3(Ti,Al)$, which provides dominant strengthening to the γ matrix. This ordered intermetallic phase provides high creep resistance and microstructural stability under thermomechanical loading, making it essential for advanced aerospace applications.

In LP-DED NASA HR-1, the primary microstructural evolution during aging is the precipitation of γ′ particles within the γ matrix. The size, morphology, and distribution of these γ′ precipitates are highly sensitive to the aging parameters. Optimizing these parameters is essential to balance strength and ductility, as well as to minimize the susceptibility of hydrogen environment embrittlement during service.

TEM was employed to characterize the γ′ precipitates. A STEM-HAADF (scanning transmission electron microscopy high-angle annular dark-field) micrograph and a corresponding selected area electron diffraction (SAED) pattern shown in Figure 27 reveal uniformly distributed, fine γ′ precipitates in the 2-step aged specimen. These particles are predominantly spherical, with mean diameters ranging from 5 to 10 nm. Their refined size and uniform dispersion suggest a well-controlled aging process. Notably, the γ′ morphology and distribution in LP-DED NASA HR-1 are comparable to those observed in its wrought counterpart[1], indicating that additive manufacturing, when paired with optimized post-processing, can yield microstructures equivalent in quality to conventionally processed materials.

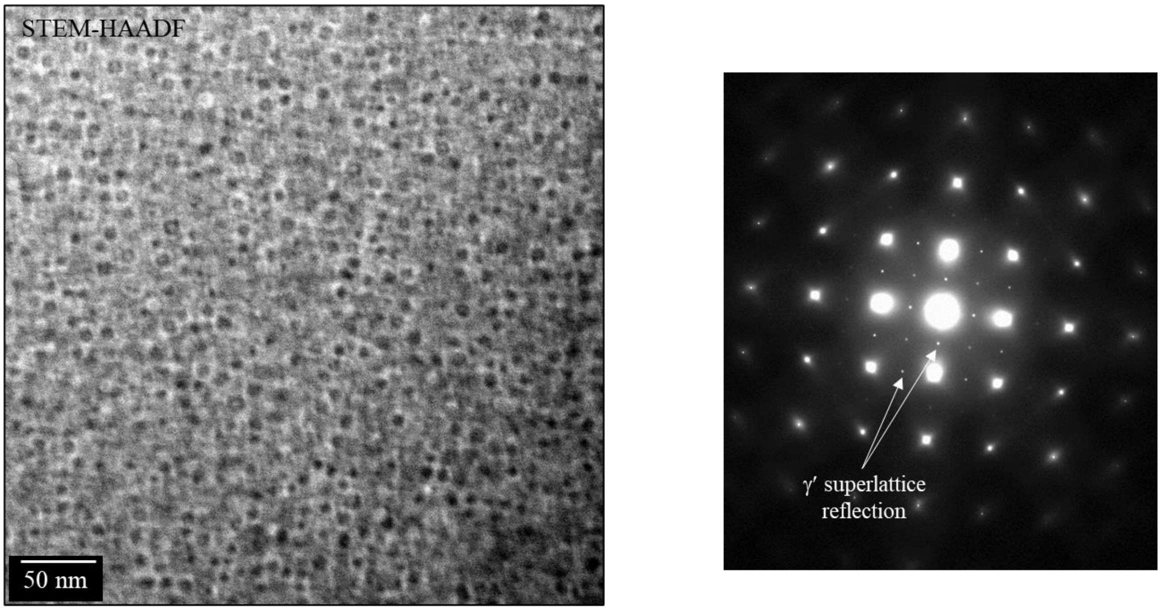

(a) (b)

Figure 27. (a) STEM-HAADF image showing fine γ′ precipitates in the two-step aged specimen. (b) Selected area diffraction pattern (SADP) taken along the [100] zone axis, showing γ′ superlattice reflections (indicated by arrows).

Further confirmation of the γ′ structure was obtained via high-resolution transmission electron microscopy (HRTEM), as shown in Figure 28. The lattice image and its corresponding Fast Fourier Transform (FFT) confirm the γ′ precipitates are nearly spherical with particle diameters close to 5 nm, underscoring the fine scale of precipitation achieved through the 2-step aging treatment.

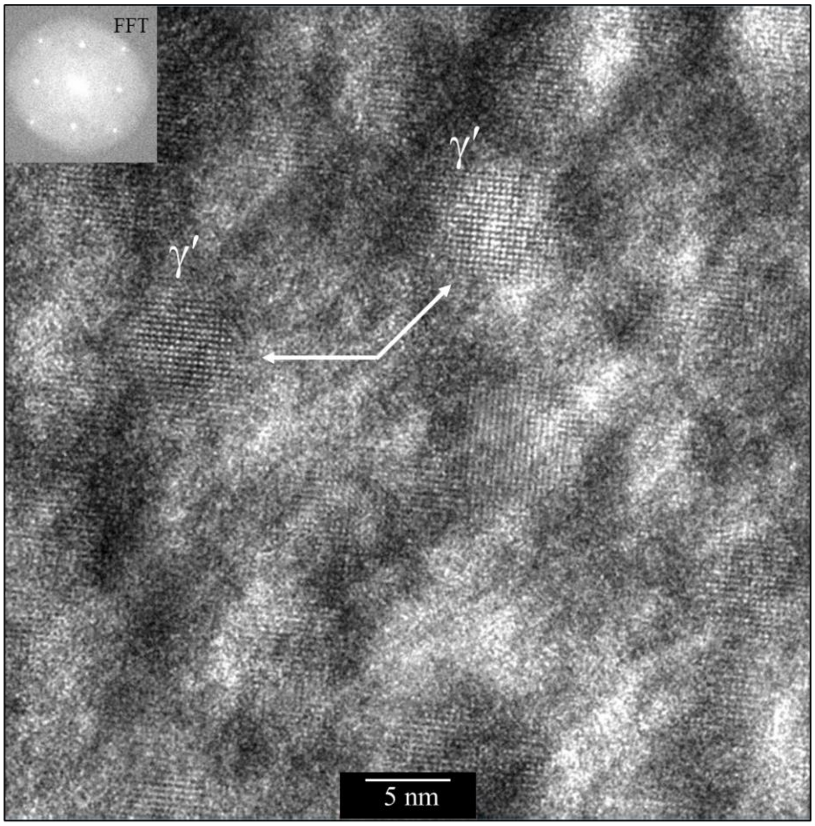

Figure 28. STEM-HAADF lattice image and corresponding FFT showing fine γ′ precipitates in LP-DED NASA HR-1. Most γ′ precipitates appear spherical with diameters around 5 nm in the two-step aged condition.

This 2-step aging heat treatment was specifically designed to mitigate microsegregation and suppress grain-boundary η-phase formation, which can be more pronounced in AM materials. Grain boundaries in the aged LP-DED NASA HR-1 specimens appear clean under both optical and scanning electron microscopy, and the detrimental η phase was not detected at this resolution. However, TEM analysis revealed the presence of nanoscale disc-shaped η′ precipitates at some grain boundaries (Figure 29). These precipitates are 50 to 80 nm in length and were only observed sporadically, suggesting partial suppression of η-phase formation, but not complete elimination.

The presence of nanoscale η-phase is concerning due to its potential impact on HEE resistance. Intergranular η precipitates can act as preferential crack initiation sites , particularly under hydrogen exposure at ambient temperature. As shown in the phase diagram (Figure 5), the η phase remains stable up to ~2000 °F (1093.33 °C) at a Ti concentration of 2.4 wt%. This suggests that the standard solution annealing treatment of 1950 °F (1065.56 °C) for 1 hour may be insufficient to fully dissolve η phase that forms during prior homogenization at 2125 °F (1162.78 °C). Consequently, achieving full dissolution of η precipitates likely requires solution annealing at temperatures above 2000 °F (1093.33 °C). These findings highlight the importance of thermodynamically informed heat treatment design to optimize both mechanical performance and environmental resistance to hydrogen embrittlement in additively manufactured HR-1 components.

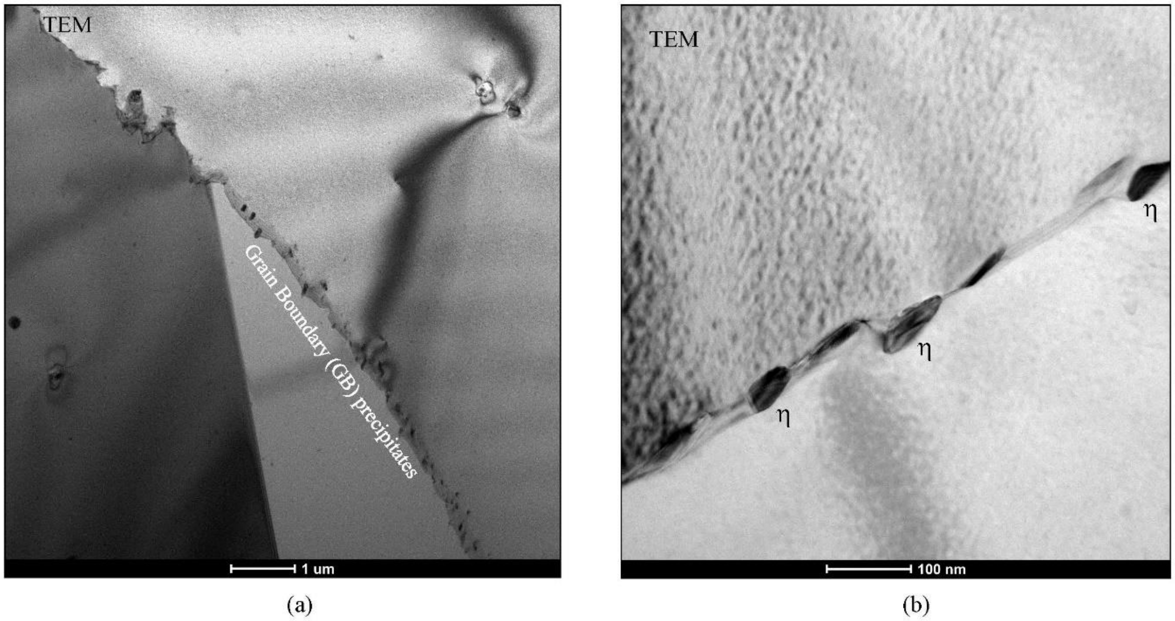

Figure 29. (a) Small precipitates observed at some grain boundaries. (b) These grain-boundary precipitates were identified as η phase (Ni_3Ti), exhibiting a disc-shaped morphology with lengths ranging from 50 to 80 nm.

3.6 Key Mechanical Properties

LREs operate under extreme conditions, with temperatures ranging from cryogenic liquid hydrogen (–423 °F [–252.78 °C]) to combustion gases exceeding 6000 °F (3315.56 °C). Structural components—particularly regeneratively cooled nozzles—often feature very thin walls that must withstand severe thermal shocks during transients and large temperature gradients during steady-state operation. These conditions, combined with prolonged exposure to both liquid and gaseous hydrogen, create an exceptionally demanding service environment. Materials for such applications must resist HEE while also meeting stringent requirements for tensile strength, ductility, LCF resistance, and thermal conductivity[6]. LP-DED NASA HR-1 was specifically developed for regeneratively cooled nozzle applications using hydrogen propellants. The alloy exhibits excellent resistance to high-pressure hydrogen-induced embrittlement and provides a balanced combination of strength, ductility, LCF resistance, HEE resistance, and thermal conductivity—making it ideally suited for advanced LRE structures[8].

3.6.1 Temperature Dependent Tensile Properties

The temperature-dependent tensile behavior of LP-DED NASA HR-1 was evaluated using specimens subjected to two aging treatments:

- **1-step aging:** 1325 °F (718.33 °C) for 16 h
- **2-step aging:** 1275 °F (690.56 °C) for 16 h followed by 1150 °F (621.11 °C) for 16 h

Table 4 summarizes the mechanical properties at test temperatures ranging from –320 °F (–195.56 °C) to 1400 °F (760 °C) [6]. Both yield strength (YS) and ultimate tensile strength (UTS) gradually decrease with increasing temperature from room temperature to 1200 °F (648.89 °C). At –320 °F (–195.56 °C), the alloy exhibits excellent ductility, with fracture elongations of 45–49%. At room temperature, elongation decreases slightly to 35–41% but remains high, with good ductility retained up to 1200 °F (648.89 °C).

The strain hardening exponent (n), derived from true stress–strain data, also declines progressively with temperature. This reduction in *n* correlates with the observed drop in fracture elongation, reflecting the strong connection between strain hardening and ductility. A higher *n* value promotes more uniform plastic deformation and delays localized necking, resulting in higher elongation. As *n* decreases at elevated temperatures, strain localizes more readily, leading to lower ductility.

The UTS/YS ratio follows a similar decreasing trend, indicating a reduced work-hardening capacity at higher temperatures. Beyond 1200 °F (648.89 °C), a sharp drop in strength, ductility, and strain-hardening behavior is observed, with properties significantly degraded at 1300 °F (704.44 °C) and 1400 °F (760 °C). Based on these results, LP-DED NASA HR-1 is recommended for structural applications up to 1200 °F (648.89 °C), where it maintains a favorable balance of strength, ductility, and strain-hardening capacity.

Table 4. Summary of tensile properties for LP-DED NASA HR-1 as a function of testing temperature from -320 °F (–195.56 °C) to 1400 °F (760 °C) [6]. For each aging condition, the tensile properties at a given test temperature are reported as the mean of five independent samples.

Laser Power & Sample Configuration	Aging Treatment	Tensile test temperature (°F)	Yield Stress (ksi)	Tensile Stress (ksi)	Fracture Elongation (%)	UTS/YS Ratio	Strain hardening exponent (n)
1070 W - round bar (0.6" diameter)	1-step	-320	106.70	205.37	44.67	1.92	0.291
	2-step		92.97	202.57	48.62	2.18	0.334
	1-step	RT	89.09	162.15	34.78	1.82	0.224
	2-step		77.28	153.91	41.36	1.99	0.283
	1-step	400	85.58	148.02	31.20	1.73	0.232
	2-step		77.84	143.32	35.60	1.84	0.254
	1-step	800	83.70	135.54	33.00	1.62	0.218
	2-step		76.10	130.36	36.60	1.71	0.234
	1-step	1000	82.58	131.12	31.40	1.59	0.210
	2-step		75.12	123.68	36.20	1.65	0.220
	1-step	1100	82.90	130.64	28.00	1.59	0.211
	2-step		73.22	120.22	33.20	1.65	0.226
	1-step	1200	85.95	123.65	22.83	1.44	0.168
	2-step		72.30	109.51	27.42	1.51	0.187
	1-step	1300	80.02	89.72	7.60	1.12	0.096
	2-step		69.84	80.50	10.20	1.15	0.111
	1-step	1400	69.38	73.96	7.40	1.07	0.080
	2-step		63.24	71.52	9.80	1.13	0.111

Aging treatment 1: 1325 °F/16h (718.33 °C/16h)
Aging treatment 2: 1275 °F/16h + 1150 °F/16h (690.56 °C/16h + 621.11 °C/16h) (32h total)

Figure 30 compares the tensile properties of LP-DED NASA HR-1 with those of its wrought counterpart. As shown, the wrought alloy consistently exhibits higher strength across all test temperatures. This strength advantage is primarily attributed to its higher titanium content (2.8%), which promotes a greater volume fraction of the γ' (Ni_3Ti) strengthening phase. In contrast, the LP-DED variant contains only 2.4% Ti, resulting in reduced γ' precipitation. This decrease in strength is an expected tradeoff associated with the chemistry reformulation designed to enable successful LP-DED processing and to optimize five key material properties: tensile strength, ductility, LCF resistance, hydrogen embrittlement resistance, and thermal conductivity[6].

Despite its lower strength, LP-DED NASA HR-1 demonstrates significantly improved ductility. Transitioning from a conventional single-step aging cycle to a lower-temperature, two-step aging treatment further enhances its ductility. Compared with the wrought alloy, the LP-DED material processed with two-step aging shows substantial increases in fracture elongation:

- From 29% to 48.6% at –320 °F (–195.56 °C)
- From 23% to 41.4% at room temperature
- From 18% to 27.4% at 1200 °F (648.89 °C)

This exceptional ductility reflects the optimized balance between alloy composition and heat treatment—tailored specifically for the LP-DED process and LRE structural applications[6].

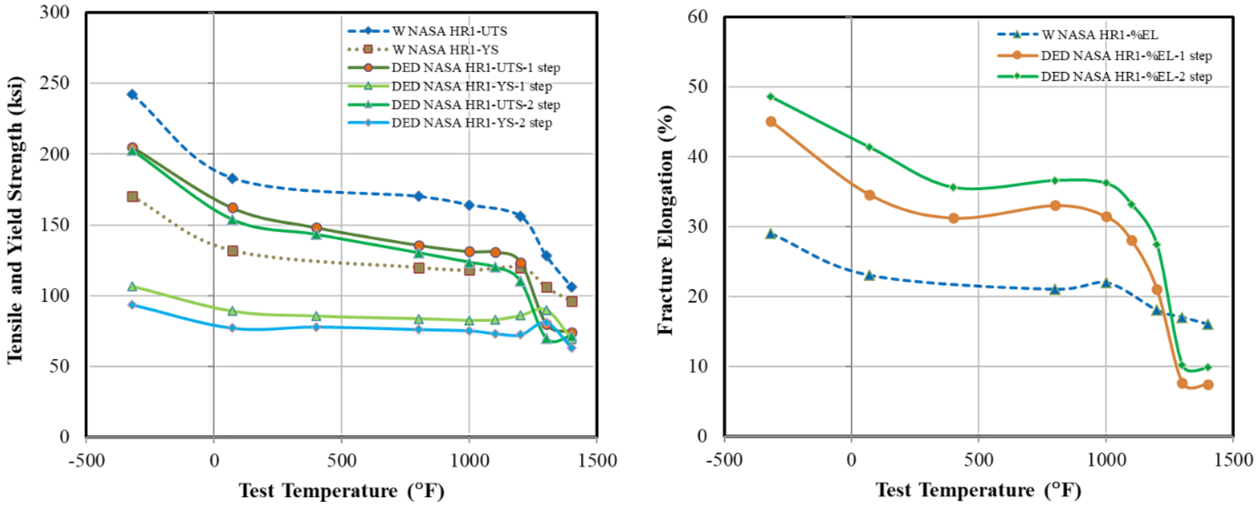

(a)

(b)

Figure 30. Comparison of (a) ultimate tensile strength and yield strength, and (b) fracture elongation of LP-DED and wrought NASA HR-1 as a function of test temperature, ranging from liquid nitrogen temperature (–320 °F [–195.56 °C]) to 1400 °F (760 °C).

3.6.2 LOW CYCLE FATIGUE (LCF) Properties In Ambient Air

In addition to tensile properties, LCF performance must be considered when designing components for LRE applications. Fully reversed tension–compression LCF tests were conducted in ambient air at room temperature using a strain ratio (R) of –1 and total strain ranges of 1% and 2%. Specimens were aged using either a 1-step or 2-step aging treatment.

Table 5 summarizes key LCF results, including inelastic strain at half-life (N_h), cycles to crack initiation (N_i), and cycles to failure (N_f). While the aging treatment has minimal impact on the inelastic strain at N_h, it has a notable influence on fatigue life. At 1% total strain, the 2-step aged specimens exhibit a 30–50% increase in total fatigue life (N_f) compared to the 1-step aged condition. Crack initiation life (N_i) is also significantly longer in the 2-step aged specimens. This improvement is consistent with tensile results showing enhanced ductility and strain hardening capacity, both of which are critical for LCF-resistant components such as LRE nozzles.

At a total strain range of 2%, the effect of aging treatment is less pronounced. The 2-step aged condition shows a moderate 15–20% increase in total fatigue life and a 10–15% increase in crack initiation life relative to the 1-step aged condition. This reduced benefit at higher strain amplitude reflects the increased dominance of plastic deformation and damage accumulation early in life. At higher strain amplitudes, the strain energy per cycle and plastic damage accumulates rapidly, overwhelming microstructural advantages such as increased ductility or refined γ′ distribution introduced by the 2-step aging treatment.

Table 5. Room temperature LCF test results for LP-DED NASA HR-1. Tests were conducted in ambient air at total strain ranges of 1% and 2%, using a strain ratio of R = –1.

Material	Environment	Strain range	Aging treatment	Specimen ID	Inelastic strain at N_h (%)	Cycles to crack initiation (N_i)	Cycles to completion (N_f)
DED NASA HR-1	Ambient	-0.5% to 0.5%	1325 °F/16h (718.33 °C/16h)	34	0.35	7,545	8,318
				104	0.337	4,794	6,600
				105	0.353	4,601	5,054
			1275 °F/16h + 1150 °F/16h (690.56 °C/16h + 621.11 °C/16h)	4	0.322	9,279	11,765
				5	0.364	6,957	7,581
				68	0.359	8,551	10,492
		-1% to 1%	1325 °F/16h (718.33 °C/16h)	121	1.205	813	899
				122	1.194	764	828
				123	1.172	860	898
			1275 °F/16h + 1150 °F/16h (690.56 °C/16h + 621.11 °C/16h)	21	1.189	897	981
				22	1.22	827	880
				23	1.227	1,121	1,298

A comparison of LCF life between LP-DED and wrought NASA HR-1 was conducted to evaluate the impact of the LP-DED process on fatigue behavior. LP-DED specimens were aged using either a 1-step or 2-step heat treatment, while wrought specimens were aged using the standard 1-step cycle (1325 °F (718.33 °C) for 16 hours). As shown in Figure 31, the LCF strain-life curves for LP-DED and wrought NASA HR-1 are generally comparable.

At a total strain of 1%, the LCF life of LP-DED specimens ranged from 5,054 to 8,318 cycles for the 1-step aged condition, and from 7,581 to 11,765 cycles for the 2-step aged condition. Wrought NASA HR-1 exhibited a slightly longer life of approximately 12,500 cycles. At a total strain of 2%, the LCF life of LP-DED specimens ranged from 828 to 898 cycles (1-step) and 880 to 1,298 cycles (2-step), while the wrought alloy reached approximately 1,020 cycles.

These results demonstrate that LP-DED is a viable manufacturing route for NASA HR-1 components subjected to severe reversed strain cycling, such as LRE nozzles. The excellent LCF performance of LP-DED NASA HR-1 is attributed to its high ductility and strain-hardening capacity, which promote uniform plastic deformation and delay crack initiation.

Although LP-DED NASA HR-1 is significantly more ductile than the wrought counterpart, the LCF life of both materials is comparable. This outcome reflects the complex interaction between global ductility, microstructural stability, and damage tolerance under cyclic loading. The enhanced ductility of LP-DED material helps accommodate plastic strain more uniformly, reducing local stress concentrations and delaying fatigue crack initiation. However, process-induced microstructural features, such as residual porosity or local texture, can act as preferential crack initiation sites, especially under high cyclic strain. In contrast, the wrought material, while less ductile, benefits from a more homogeneous and defect-free microstructure that enhances fatigue resistance. The comparable LCF life observed in both materials therefore reflects a balance between these competing effects.

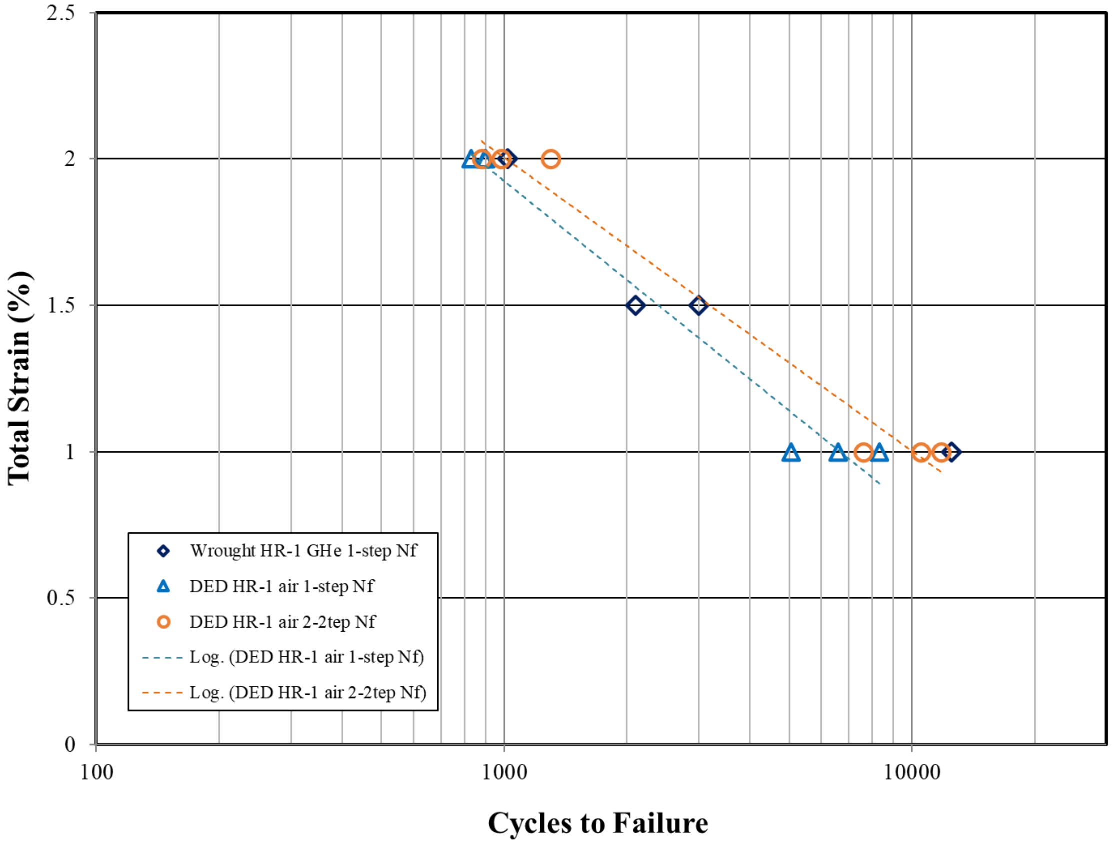

Figure 31. Comparison of LCF strain-life curves for LP-DED and wrought NASA HR-1. LP-DED specimens were heat treated using either a one-step or two-step aging cycle, while wrought specimens underwent the standard one-step aging at 1325 °F (718.33 °C) for 16 hours.

3.6.3 Tensile Properties In High Pressure Hydrogen Environment

To assess the HEE susceptibility of LP-DED NASA HR-1, tensile tests were conducted at room temperature in 5 ksi high-pressure gaseous hydrogen. HEE describes the degradation of mechanical properties that can occur when a material is exposed to high-pressure hydrogen under stress, with peak susceptibility typically occurring near ambient temperature. A common method for evaluating HEE is to compare tensile ductility in hydrogen with that obtained in an inert environment such as nitrogen or helium[28].

LP-DED specimens were heat treated using two aging cycles: a standard one-step aging at 1325 °F (718.33 °C) for 16 hours, and a two-step aging at 1275 °F (690.56 °C) for 16 hours followed by 1150 °F (621.11 °C) for 16 hours. Baseline tensile tests were performed in 5 ksi nitrogen or helium (inert gas) at a strain rate of 0.05 in/in/min. For hydrogen testing, the strain rate was reduced to 0.005 in/in/min to increase sensitivity to embrittlement effects. Table 6 summarizes the tensile properties of LP-DED NASA HR-1 in nitrogen and hydrogen, along with reference data for wrought NASA HR-1 tested in helium and hydrogen.

As shown in Table 6, the two-step aged LP-DED NASA HR-1 exhibited essentially no degradation in tensile properties in hydrogen, indicating very low HEE susceptibility. Fracture elongation in hydrogen was comparable to that in helium or nitrogen. Additionally, in high-pressure nitrogen, the two-step aged condition showed lower strength but significantly greater ductility than the one-step aged condition.

Compared with wrought NASA HR-1, the LP-DED material demonstrated superior ductility but lower strength in hydrogen. The two-step aged LP-DED samples achieved a fracture elongation of 41.6% in hydrogen, nearly double that of wrought NASA HR-1, which exhibited only 23.4% elongation. While the yield and ultimate tensile strengths of the LP-DED material (76.0 ksi and 154.3 ksi) were lower than those of wrought NASA HR-1 (128.8 ksi and 175.4 ksi), the enhanced ductility suggests that the LP-DED process, when paired with optimized aging treatments, can improve hydrogen resistance and produce a material with excellent tensile ductility in high-pressure hydrogen environments. This reflects a common trade-off in alloy design: moderate reductions in strength can sometimes significantly improve resistance to HEE by promoting more uniform deformation and delaying crack initiation.

Table 6. Average tensile properties from tests performed in high-pressure nitrogen, helium, and hydrogen environments. For each aging condition, the tensile properties under a given test environment are reported as the mean of three independent samples.

Material	Aging Treatment	Strain rate (in/in/min)	Test Environment	Yield Stress (ksi)	Ultimate Tensile Stress (ksi)	Ductility (% EL)
LP-DED NASA HR-1	1-step	0.05	5 ksi GN_2	102.08	170.17	34.5
		0.005	5 ksi GH_2	-	-	-
LP-DED NASA HR-1	2-step	0.01	5 ksi GN_2	76.53	152.92	40.54
		0.005	5 ksi GH_2	76.03	154.34	41.61
Wrought NASA HR-1	1-step	0.05	5 ksi GHe	136.93	183.07	23.57
		0.005	5 ksi GH_2	128.83	175.37	23.4

To further quantify HEE resistance, Table 7 presents the ratios of YS, UTS, and fracture elongation in hydrogen relative to values in inert gas (GN_2 or GHe) for both LP-DED and wrought NASA HR-1. At a strain rate of 0.005 in/in/min, the GH_2/GN_2 ductility ratio for LP-DED NASA HR-1 was 1.03—comparable to the wrought alloy's 0.99—but with significantly higher absolute ductility in hydrogen (41.6% vs. 23.4%). Strength retention was also slightly better for LP-DED, with GH_2/GN_2 YS and UTS ratios of 0.99 and 1.01, respectively, compared to 0.94 and 0.96 for the wrought material.

The improved hydrogen performance of LP-DED NASA HR-1 is likely associated with its lower baseline strength and higher strain hardening capacity. Higher-strength materials tend to generate greater stress intensities at crack tips during plastic deformation, which promotes hydrogen-assisted crack initiation and growth. In contrast, materials with greater strain hardening can distribute plastic strain more uniformly, delaying crack propagation and reducing susceptibility to hydrogen environment embrittlement.

Table 7. GH_2/inert gas ratios of yield strength (YS), ultimate tensile strength (UTS), and ductility (fracture elongation) for LP-DED and wrought NASA HR-1.

Material	**Heat Treatment**	**Surface Finish**	**Strain Rate**	**YS ratio (GH_2/GN_2)**	**UTS ratio (GH_2/GN_2)**	**Ductility ratio (GH_2/GN_2)**
LP-DED NASA HR-1	2-step aging	LSG	0.005 in/in/min	0.99	1.01	1.03
Wrought NASA HR-1	1-step aging	LCG	0.005 in/in/min	0.94	0.96	0.99

Figure 32 compares fracture elongation for LP-DED and wrought NASA HR-1 tested in inert gas and high-pressure hydrogen environments. Both alloys exhibit excellent resistance to hydrogen embrittlement, as evidenced by the minimal difference in elongation between inert and hydrogen environments. However, LP-DED NASA HR-1 is significantly more ductile than the wrought alloy. In hydrogen, the LP-DED material achieved 41.6% elongation, nearly twice that of the wrought material, which reached only 23.4%.

In summary, LP-DED NASA HR-1, particularly in the two-step aged condition—shows excellent resistance to hydrogen environment embrittlement. The combination of high ductility, strong strength retention, and minimal environmental degradation highlights the effectiveness of additive manufacturing coupled with optimized heat treatment. These results demonstrate the strong potential of LP-DED NASA HR-1 for demanding applications such as liquid rocket engines, where both mechanical performance and hydrogen compatibility are critical.

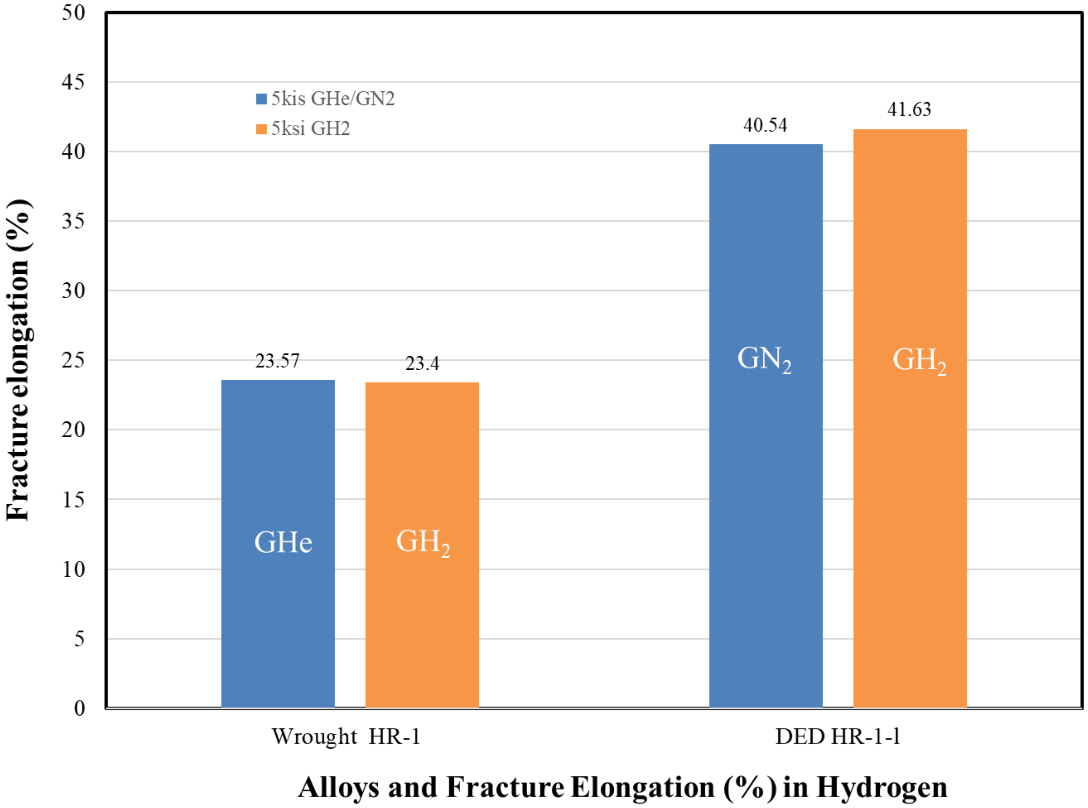

Figure 32. Comparison of HEE susceptibility based on fracture elongation for LP-DED and wrought NASA HR-1 tested in high-pressure hydrogen and inert gas environments.

3.6.4 Low Cycle Fatigue (LCF) Properties In High Pressure Gaseous Hydrogen (GH_2) Environment

LCF is the primary life-limiting mechanism for LRE nozzles. Exposure to a high-pressure GH_2 environment can significantly degrade the LCF performance in materials that are susceptible to HEE. Strain-controlled LCF testing is generally more sensitive to HEE effects than load-controlled high cycle fatigue (HCF) testing, as it directly captures hydrogen-assisted damage during cyclic plastic deformation. For most superalloys, the greatest reduction in LCF life in high-pressure hydrogen occurs near room temperature.

To assess the effect of hydrogen on fatigue crack initiation and total fatigue life, Strain-controlled LCF tests were conducted at room temperature in 5 ksi GH_2 using a total strain range of 2% and a strain ratio of $R = -1$. The 2% strain range was selected based on the projected maximum total strains in channel wall nozzles during hot-fire testing, which typically approach ~2%.

Table 8 summarizes the LCF test results, including inelastic strain amplitude, cycles to crack initiation (N_i), and cycles to failure (N_f). Specimens were heat treated using either a one-step or a two-step aging cycle. A modest increase in inelastic strain was observed with the two-step aging treatment. Specimens subjected to the two-step cycle showed improved fatigue resistance, with longer crack initiation life (N_i = 860–865 cycles) compared to the one-step aged specimens (N_i = 660–760 cycles). A modest improvement in total fatigue life (N_f) was also observed for the two-step aged condition.

Table 8. LCF test results for LP-DED NASA HR-1 in 5 ksi high pressure hydrogen environment at room temperature.

Material	Environment	Strain range	Aging treatment	Specimen ID	Inelastic strain at N_h (%)	Cycles to crack initiation (N_i)	Cycles to failure (N_f)
LP-DED NASA HR-1	5ksi GH_2, RT	-1% to 1%	1325 °F/16h	38	1.25	≈ 660	789
				39	1.25	≈ 760	918
				40	1.26	≈ 750	922
			1275 °F/16h + 1150 °F/16h	73	1.31	≈ 860	878
				74	1.33	≈ 865	884
				75	1.34	≈ 865	993

3.6.5 Comparison of Low Cycle Fatigue (LCF) Behavior In Air and Hydrogen

LCF testing conducted in a high-pressure hydrogen environment shows minimal degradation in the fatigue life of LP-DED NASA HR-1 compared to ambient air. As shown in Figure 33, the LCF life at a total strain range of 2% is comparable in both environments.

In the one-step aged condition, the average LCF life was 870 cycles in air and 876 cycles in hydrogen, indicating essentially no environmental effect. In the two-step aged condition, the average LCF life was 1,053 cycles in air and 918 cycles in hydrogen, representing a modest reduction in life in hydrogen. However, in both environments, the two-step aged material consistently exhibited longer LCF life than the one-step aged material.

At a 2% total strain range, the fatigue response is dominated by cyclic plastic deformation, making ductility more critical than strength in determining fatigue life. The comparable LCF lives observed in air and hydrogen indicate that LP-DED NASA HR-1 retains its cyclic deformation capability in a hydrogen environment without significant hydrogen-assisted cracking. Its high ductility and strong strain hardening capacity contribute to the extended fatigue life in both environments.

The excellent LCF performance in high-pressure hydrogen environment underscores the suitability of LP-DED NASA HR-1 for LRE components subjected to repeated thermal and mechanical loading in hydrogen-rich service environments.

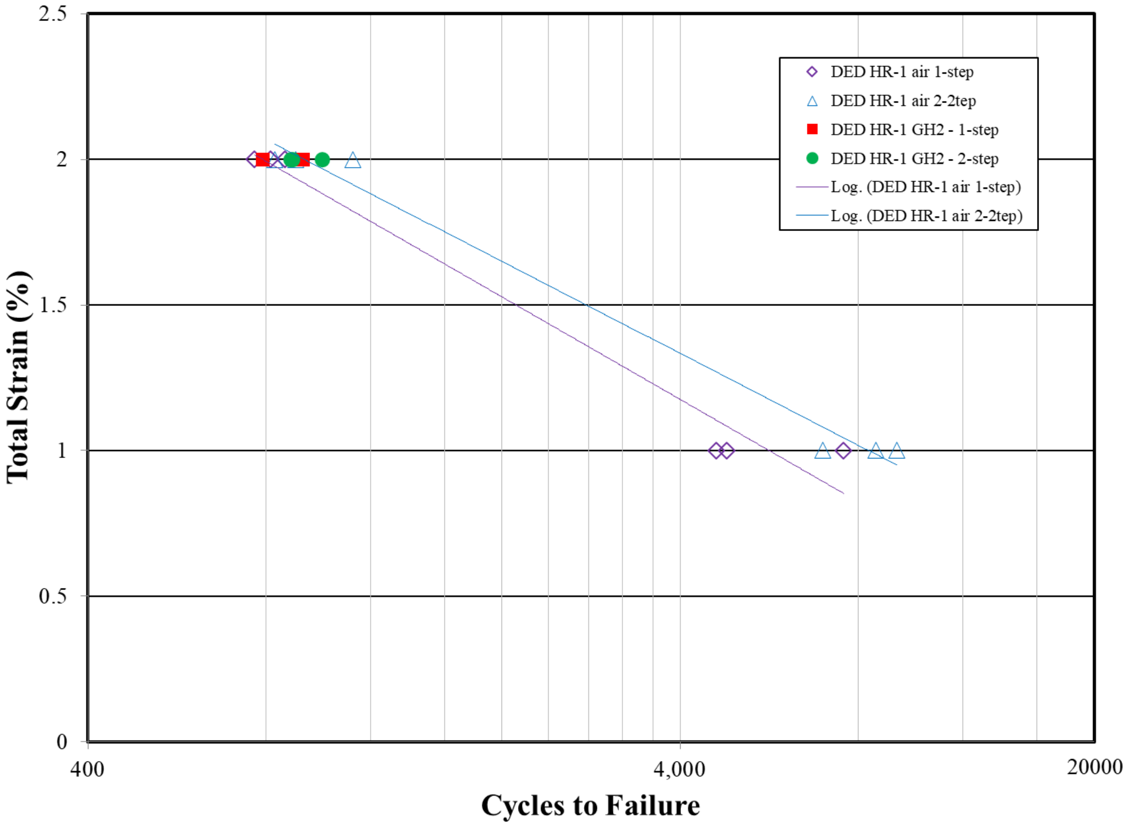

Figure 33. Comparison of low cycle fatigue (LCF) life for LP-DED NASA HR-1 tested in ambient air and 5 ksi hydrogen at room temperature. Specimens were heat treated using either a one-step or two-step aging cycle.

3.6.6 Comparison of Low Cycle Fatigue (LCF) Life In Hydrogen For Laser Powder Directed Energy Deposition (LP-DED) and Wrought NASA HR-1

Figure 34 compares the strain-controlled LCF life of wrought and LP-DED NASA HR-1 tested in a high-pressure gaseous hydrogen environment. Although wrought NASA HR-1 shows only a minor reduction in tensile fracture elongation in 5 ksi gaseous hydrogen environment, its LCF life is significantly degraded in the same environment[1]. In contrast, LP-DED NASA HR-1 exhibits minimal loss in LCF life in hydrogen.

The wrought material was heat treated using the standard one-step aging cycle (1325 °F [718.33 °C] for 16 hours). LP-DED NASA HR-1 was heat treated using either the same one-step cycle or a two-step aging cycle (1275 °F [690.56 °C] for 16 hours followed by 1150 °F [621.11 °C] for 16 hours). At a total strain range of 2%, the average LCF life in hydrogen was 876 cycles for LP-DED NASA HR-1 aged using the one-step cycle, compared to just 315 cycles for the wrought alloy. Application of the two-step aging treatment further increased the LCF life of LP-DED material to 918 cycles.

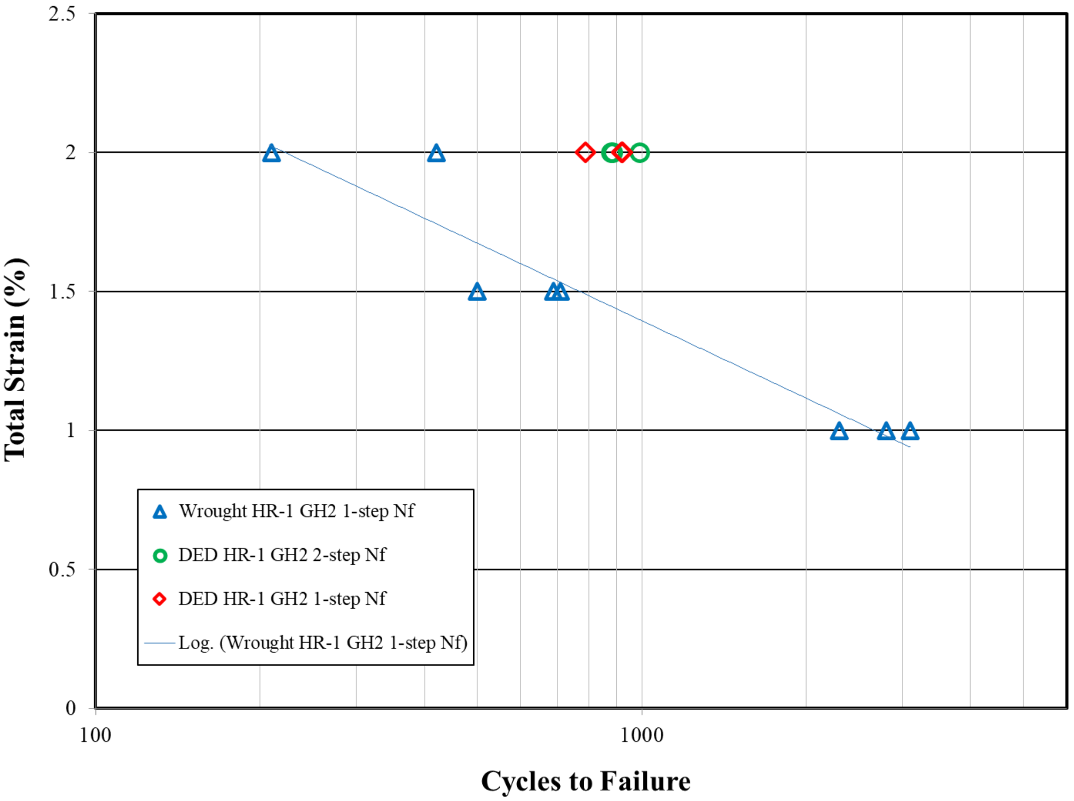

Figure 34. Effect of high-pressure hydrogen on the LCF life of LP-DED and wrought NASA HR-1. The wrought alloy was aged using a one-step cycle at 1325 °F (718.33 °C) for 16 hours. LP-DED NASA HR-1 was aged using either the same one-step cycle or a two-step cycle at 1275 °F (690.56 °C) for 16 hours followed by 1150 °F (621.11 °C) for 16 hours. In a high-pressure hydrogen environment, LP-DED NASA HR-1 exhibits significantly greater LCF resistance than the wrought alloy.

These results clearly demonstrate that LP-DED NASA HR-1 offers significantly improved LCF resistance in high-pressure hydrogen compared to its wrought counterpart. The pronounced reduction in LCF life observed in the wrought alloy, despite its relatively preserved tensile ductility, highlights the importance of evaluating strain-controlled fatigue behavior when assessing HEE susceptibility. In HEE-sensitive materials, hydrogen can significantly reduce cyclic ductility, accelerate crack initiation, and alter cyclic plastic deformation behavior, even when monotonic tensile properties appear only mildly affected[6].

Notably,, the LCF life of LP-DED NASA HR-1 in hydrogen remains comparable to its performance in air at a 2% total strain range. Typical LCF lives range from 827–1121 cycles in air and 878–893 cycles in hydrogen. This exceptional LCF performance in hydrogen underscores the strong potential of LP-DED NASA HR-1 for LRE components subjected to repeated thermal and mechanical loading in aggressive hydrogen-rich service environments.

4. SUMMARY AND CONCLUSIONS

4.1 Additive Manufacturing (AM) Feasibility

The hydrogen-resistant NASA HR-1 alloy was successfully fabricated using LP-DED. The alloy exhibits excellent printability and can be reliably built via the LP-DED process. Achieving optimal mechanical properties requires a thorough understanding of LP-DED process parameters and microstructural evolution under complex thermal histories. This study establishes key heat treatment design principles and demonstrates the utility of DSC as a practical tool of monitoring precipitate evolution during thermal processing.

4.2 Microstructure Control and Grain Recrystallization

Through appropriate post-processing heat treatments, LP-DED NASA HR-1 can develop a desirable, fully recrystallized microstructure. Stress relief at 1950 °F (1065.56 °C) for 1.5 hours promotes partial recrystallization, while subsequent homogenization at 2125 °F (1162.78 °C) for 3 hours achieves full recrystallization. Understanding phase formation and recrystallization behavior is critical for controlling the final microstructure.

4.3 Precipitation Behavior and Phase Stability

Solution annealing followed by aging treatments produce fine γ' precipitates (~5–10 nm) responsible for strengthening. Two-step aging increases the γ' volume fraction and enhances microstructural stability by delaying η-phase formation. Grain boundaries remain clean, with no η-phase observed by optical microscopy or SEM; however, occasional nanoscale η particles (50–80 nm) are detected in high-resolution TEM. The results suggest that solution annealing above 2000 °F (1093.33 °C) may be required to fully eliminate residual η phase.

4.4 HYDROGEN ENVIRONMENT EMBRITTLEMENT (HEE) RESISTANCE

Tensile testing in gaseous hydrogen confirms that LP-DED NASA HR-1 exhibits excellent resistance to hydrogen embrittlement. At a standard strain rate of 0.005 in/in/min, the alloy retains high ductility with no measurable loss in hydrogen. The tensile ductility ratio (GH_2/GN_2) matches that of wrought NASA HR-1, while the absolute ductility exceeds the wrought alloy by more than 15%, demonstrating the robustness of the AM-processed alloy in hydrogen environments.

4.5 LOW CYCLE FATIGUE (LCF) PERFORMANCE IN HYDROGEN

In the two-step aged condition, LP-DED NASA HR-1 achieves LCF performance comparable to the wrought alloy in air—and significantly better performance in high-pressure hydrogen. Its high ductility and strong strain hardening response minimize fatigue degradation in hydrogen. These properties make LP-DED NASA HR-1 a highly promising material for LRE structures subjected to cyclic thermal and mechanical loading in hydrogen-rich environments.

5. REFERENCES

1. Chen, P.S.; Panda B.; and Bhat, B.N.: "NASA HR-1, A New Hydrogen Resistant Fe-Ni Base Superalloy," in Proc. of the Fifth International Conference on the Effect of Hydrogen on the Behavior of Materials, A.W. Thompson and N.R. Moody (eds.), September 11–14, 1994, The Minerals, Metals and Materials Society, Moran, WY, pp. 1011–1020, 1996.

2. Chandler, W. T. "Hydrogen-Environment Embrittlement and Its Control in High Pressure Hydrogen/Oxygen Rocket System," Advanced Earth-to-Orbit Propulsion Technology of NASA Conference Publication 2437, no. 2, (1986).

3. Katsaleris, C.C., Chen, P.S., Grald, P.R., Protz, C.S, Jones, Z., Ellis, D.L., Evans, L. "Additive Manufacturing of NASA HR-1 for Liquid Engine Component Applications", JANNAF, (December 2019) United States.

4. Chen, P.S.; Katsarelis, C.C.; Medders, W.M.; and Gradl, P.R.: "Segregation Evolution and Diffusion of Titanium in DED NASA HR-1", NASA/TM 20210013649, May 2021.

5. Gradl, Paul R., Thomas W. Teasley, Christopher S. Protz, Colton C. Katsarelis, and Po-Shou Chen. "Process Development and Hot-fire Testing of Additively Manufactured NASA HR-1 for Liquid Rocket Engine Applications," AIAA Propulsion and Energy Forum (2021).

6. Chen, P.S., Katsarelis, C.C, Medders, W.M., Gradl, P.R., Su, C.H. "Development of Directed Energy Deposited NASA HR-1 to Optimize Properties for Liquid Rocket Engine Applications," NASA/TM 20230006075, April 2023.

7. Chen, P.S., Fullen, M.D., Watwood, W.C., Rupp, B.L., Medders, W.M, Colton, C.C., Gradl, P.R. "Effects of Strain Rate and Surface Finish on Tensile Properties in High Pressure Hydrogen - A Case Study for LP-DED NASA HR-1," NASA/TM 20230008831, June 2023.

8. Gradl, P.R., Mireles, O.R., Katsarelis, C.C., Smith, T.M., Sowards, J.W., Park, A.M., Chen, P.S., Tinker, D.C., Protz, C.S. Teasley, T.W., Ellis, D.L., Kantzos, C.A. "Advancement of extreme environment additively manufactured alloys for next generation space propulsion applications," Acta Astronautica 211 (2023) 483–497

9. Gradl, P.R., Tinker, D.C., Park, A.M., Mireles, O.R., Garcia, M.B., Wilkerson, R.P., and McKinney, C.G. "Robust Metal Additive Manufacturing Process Selection and Development for Aerospace Components," Journal of Materials Engineering and Performance. Springer (2021). https://doi.org/10.1007/s11665-022-06850-0.

10. Gradl, P. R. "Rapid Fabrication Techniques for Liquid Rocket Channel Wall Nozzles." AIAA-2016-4771, Paper presented at 52nd AIAA/SAE/ASEE Joint Propulsion Conference, July 27, 2016. Salt Lake City, UT.

11. Gradl, P.R., and Protz, C.S. “Technology advancements for channel wall nozzle manufacturing in liquid rocket engines,” Acta Astronautica 174 (2020): 148-158 https://doi.org/10.1016/j.actaastro.2020.04.067.

12. Gradl, P.R., Greene, S.E., Brandsmeier, W.C, and Johnston, M.I. “Hot-fire Testing and Large-scale Deposition Manufacturing Development Supporting Liquid Rocket Engine Channel Wall Nozzle Fabrication,” Paper presented at 65th JANNAF Propulsion Meeting/10th Liquid Propulsion Subcommittee, May 21–24, 2018. Long Beach, CA.

13. Gradl, P.R., Greene, S.E., Portz, C.C., Bullard, D.B., Buzzell, J.C., Garcia, C.P., Wood, J., Osbourne, R.J., Hulka, J.R., and Cooper, K.G. “Additive Manufacturing of Liquid Rocket Engine Combustion Devices: A Summary of Process Developments and Hot-Fire Testing Results,” 54th AIAA/SAE/ASEE Joint Propulsion Conference. Cincinnati, OH: AIAA Propulsion and Energy Forum, July 9-12, 2018. AIAA 2018–4625.

14. Gradl, P.R., Protz, C.S., and Wammen, T.G. “Additive Manufacturing Development and Hot-fire Testing of Liquid Rocket Channel Wall Nozzles using Blown Powder Directed Energy Deposition Inconel 625 and JBK-75 Alloys,” 55th AIAA/SAE/ASEE Joint Propulsion Conference. Indianapolis, IN: AIAA Propulsion and Energy Forum, August 19-21. AIAA-2019-4362.

15. David, S.A.; Siefert, J.A.; DuPont J.N.; and Shingledecker, P.: “Weldability and Weld Performance of Candidate Nickel Based Superalloys for Advanced Ultrasupercritical Fossil Power Plants Part I: Fundamentals”, Science and Technology of Welding and Joining, Vol. 20, No. 7, pp. 532 – 552, 2015.

16. Richard, B.F., “Age-Hardenable Superalloys”, Advanced Materials & Processes, Vol. 163, No. 6, p. 37-42, June 2005.

17. Papadaki, C., Li, W., and Korsunsky, A.M., “On the Dependence of γ' Precipitate Size in a Nickel-Based Superalloy on the Cooling Rate from Super-Solvus Temperature Heat Treatment”, Materials 2018, 11, 1528.

18. Bassini, E., Cattano, G., Marchese, G., Biamino, S., Ugues, D., Lombardi, M., Vallillo, G., and Picque, B., “Study of the Effects of Aging Treatment on Astroloy Processed via Hot Isostatic Pressing”, Materials 2019, 12, 1517.

19. Nana Kwabena Adomako, Nima Haghdadi, and Sophie Primig,” Electron and Laser-based additive manufacturing of Ni-based superalloys: A review of heterogeneities in microstructure and mechanical properties,” Materials & Design 223 (2022) 111245.

20. Neghlani, P.K.: “SLM additive manufacturing of Alloy 718 Effect of process parameters on microstructure and properties,” M.S. Thesis, University West, pp. 48, doi:10.13140/RG.2.2.25434.64963, August 2016.

21. Reza Soleimani Gilakjani[1], Seyed Hossein Razavi[1*] and Masoumeh Seifollahi[2], “The Effect of Niobium Addition on the Microstructure and Tensile Properties of Iron-Nickel Base A286 Superalloy”, Iranian Journal of Materials Science and Engineering, Vol. 18, Number 1, March 2021.

22. Fencheng, L.; Xin, L.; Gaolin, Y.; et al.: “Recrystallization and its influence on microstructures and mechanical properties of laser solid formed nickel base superalloy Inconel 718,” Rare Metals, Vol. 30, No. 1, pp. 433–438, doi:10.1007/s12598-011-0319-0, March 2011.

23. Zhang, F; Levine, L.E.; Allen, A.J.; et al.: “Effect of heat treatment on the microstructural evolution of a nickel-based superalloy additive-manufactured by laser powder bed fusion,” Acta Materialia, Vol. 152, pp. 200–214, June 2018.

24. Cao, J; Liu, F; Lin, X.; et al.: “Effect of overlap rate on recrystallization behaviors of Laser Solid Formed Inconel 718 superalloy,” Optics & Laser Technology, Vol. 45, pp. 228–235, February 2013.

25. M. Seifollahi, S.H. Razavi, Sh. Kheirandish, and S.M. Abbasi, “The Mechanism of η Phase Precipitation in A286 Superalloy During Heat Treatment, “ Journal of Materials Engineering and Performance, May 2013. JMEPEG DOI: 10.1007/s11665-013-0592-1

26. Abdul Shaafi Shaikh, “Development of a γ’ Precipitation Hardening Ni-Base Superalloy for Additive Manufacturing,” Department of Industrial and Materials Science, Chalmers University of Technology, 2018.

27. Hiromu Hisazawa[1,*], Yoshihiro Terada[2] and Masao Takeyama[3], “Morphology Evolution of γ' Precipitates during Isothermal Exposure in Wrought Ni-Based Superalloy Inconel X-750”, Materials Transactions, Vol. 58, No. 5 (2017) pp. 817 to 824.

28. Lee, Jonathan A. “Hydrogen Embrittlement”, NASA Technical Memorandum, 2016-218602.

National Aeronautics and
Space Administration
IS63
George C. Marshall Space Flight Center
Huntsville, Alabama 35812